Experimental Study of Water-Ice Phase Change Process Improvement Using Ultrasonic Energy

by

Varun Subramanian

A Thesis Presented in Partial Fulfillment
of the Requirements for the Degree
Master of Science

Approved April 2021 by the
Graduate Supervisory Committee:

Patrick Phelan, Chair
Ronald Calhoun
Konrad Rykaczewski

ARIZONA STATE UNIVERSITY

May 2021

ABSTRACT

The phase change process of freezing water is an important application in several fields such as ice making, food freezing technologies, pharmaceuticals etc. Due to the widespread usage of ice-related products, process improvements in this technology can potentially lead to substantial energy savings. After studying the freezing process of water, the supercooling phenomenon was found to occur which showed a negative effect. Therefore, ultrasound was proposed as a technique to reduce the supercooling effect and improve the heat transfer rate. An experimental study was conducted to analyze the energy expenditures in the freezing process with and without the application of ultrasound. After a set of preliminary experiments, an intermittent application of ultrasound at 10W & 3.5W power levels were found to be more effective than constant-power application, and were explored in further detail. The supercooling phenomenon was thoroughly studied through iterative experiments. It was also found that the application of ultrasound during the freezing process led to the formation of shard-like ice crystals. From the intermittent ultrasound experiments performed at 10W and 3.5W power levels, percentage energy enhancements relative to no ultrasound of 8.9% $\pm$ 12.4% and 11.9% $\pm$ 24.6% were observed, respectively.

ACKNOWLEDGMENTS

I would like to give thanks to Dr. Patrick Phelan for his continual mentorship and guidance over the course of this study. I would also like to thank Dr. Konrad Rykaczewski and Dr. Ronald Calhoun for being a part of my committee team.

I would also like to specially thank Hooman Daghooghi Mobarakeh for his constant help and counsel throughout this research.

Finally, I wish to convey my deepest gratitude to my family and friends who have been a constant source of support for me through this journey.

TABLE OF CONTENTS

Page

LIST OF TABLES

LIST OF FIGURES

Figure Page

NOMENCLATURE

Atmospheric pressure	P_{atm} [atm]
Characteristic length	L_c [m]
Coefficient of volume expansion	β $[T^{-1}]$
Convective heat transfer coefficient	h_{conv} $[W\ m^{-2}K^{-1}]$
Cooling energy input	$E\ [J]$
Cosine phase angle between the voltage and current	$cos\theta$
Cylinder diameter	D [m]
Density	ρ $[kg\ m^3]$
Density of air at the far field	$\rho_{a,\infty}$ $[kg\ m^3]$
Density of air near the surface	$\rho_{a,surface}$ $[kg\ m^3]$
Density of vapor at the far field	$\rho_{v,\infty}$ $[kg\ m^3]$
Density of vapor near the surface	$\rho_{v,surface}$ $[kg\ m^3]$
Diffusion coefficient	D_{H_2O-Air} $[m^2\ s^{-1}]$
Dynamic viscosity	μ $[kg\ m^{-1}\ s^{-1}]$
Far field temperature	$T_\infty [K]$

Far field vapor pressure of air	$P_{v,\infty}\ [KPa]$
Film temperature	$T_f\ [K]$
Gas constant of air	$R_a\ [kJ\ kg^{-1}\ K^{-1}]$
Gas constant of vapor	$R_v\ [kJ\ kg^{-1}\ K^{-1}]$
Gravitational acceleration	$g\ [m\ s^{-2}]$
Heat capacity	$C_p\ \ [J\ K^{-1}]$
Heat transfer coefficient	$h\ [W\ m^{-2}K^{-1}]$
Heat transfer due to mass diffusion	$Q_m\ [W]$
Heat transfer rate	$Q[W]$
Inlet temperature	$T_{\text{in}}\ [K]$
Kinematic viscosity	$v\ [m^2\ s^{-1}]$
Mass flow rate	$\dot{m}\ [kg\ s^{-1}]$
Mass transfer coefficient	$h_{mass}\ [m\ s^{-1}]$
Non-Ultrasound	NUS
Nusselt number	Nu
Outlet temperature	$T_{\text{out}}\ [K]$

Dry air pressure at the far field	$P_{a,\infty}$ $[KPa]$
Dry air pressure near the surface	$P_{a,surface}$ $[KPa]$
Power supplied to transducer	P_{US} $[W]$
Prandtl number	Pr
Rate of mass diffusion	m_v $[kg\ hr^{-1}]$
Rayleigh number	Ra
Relative humidity	$\emptyset$
Root mean square alternating current	I_{rms} $[A]$
Root mean square voltage	V_{rms} [V]
Schmidt number	Sc
Sherwood number	Sh
Specific enthalpy of water	h_{fg} $[J\ kg^{-1}\ K^{-1}]$
Surface area	A_s $[m^2]$
Surface temperature	Ts $[K]$
Temperature difference	ΔT $[K]$
Thermal conductivity	k $[W\ m^{-1}\ K^{-1}]]$

Thermal diffusivity	$\alpha\ [m^2\ s^{-1}]$
Thermal mass of the cooling module	$Q_{thermal\ mass}\ [J\ K^{-1}]$
Total density of air-vapor mixture at the far field	$\rho_\infty\ [kg\ m^3]$
Ultrasound	US
Vapor pressure near the surface	$P_{v,surface}\ [KPa]$
Vapor saturation pressure	$P_{sat,\infty}\ [KPa]$

CHAPTER 1

INTRODUCTION

The process of freezing water is an important application in a variety of fields such as ice making, food freezing technologies, pharmaceuticals etc. With an abundant and widespread need for ice-related products in both the commercial and industrial sectors, it becomes necessary to ensure that the phase change process of freezing water to ice is done as energy efficiently as possible.

1.1. Energy Impact of Freezing Processes

A literature review was conducted on the various energy impact studies that were performed on refrigeration equipment used for freezing applications in the United States. A study conducted by the Department of Energy in 2009 estimated that a total of 1.23 Quads of primary energy per year was used in commercial refrigeration equipment under which ice machines exclusively accounted for 0.28 Quads/yr of primary energy [1]. On a commercial scale, the combined value of ice shipments in the United States was $595,487,000 according to the census of 2002 [2]. Fisher et al. conducted an independent study and suggested that the total inventory of ice machines in the USA was between 2.5 to 3 million units [3]. Yashar et al. investigated the energy consumption of automatic ice makers installed in domestic refrigerators and found that the range of tested products consumed between 0.249 to 0.652 kWh per kilogram of ice, which causes approximately 12% - 20% of additional energy consumption in an individual refrigerator [4]. Therefore, it can be observed that there are considerable energy savings potential in this area.

1.2. Supercooling

A literature review was conducted on the freezing process of water, and a phenomenon known as supercooling was found to occur which had a negative impact on the phase change process.

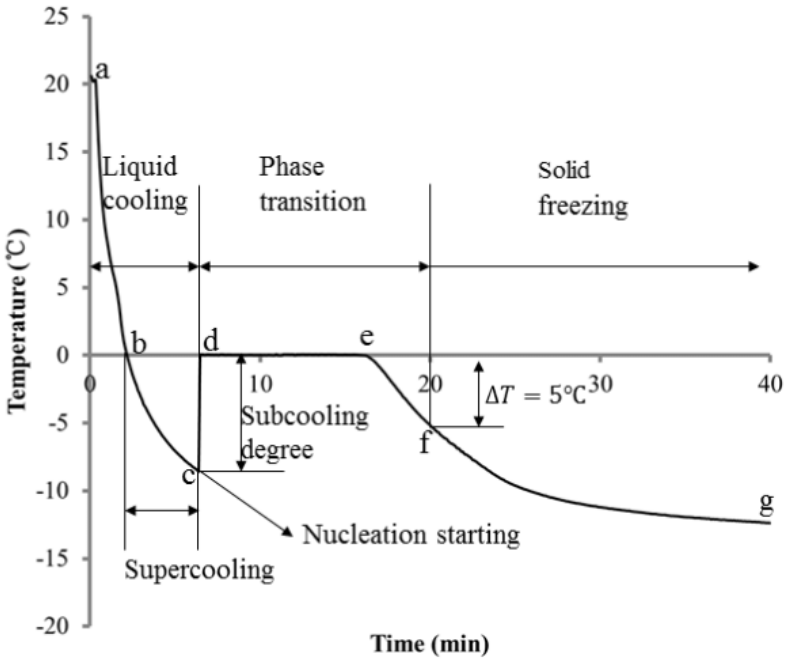

Figure 1.1: Cooling curve of water depicting supercooling phenomenon.[5]

Supercooling (or undercooling) is the process of decreasing the temperature of a fluid below its melting point while it remains in a liquid state as indicated by Figure 1.1 [6]. This occurs when there is an absence of a seed crystal or nucleus which can initiate the formation of a crystal structure [7]. Supercooling was first discovered in 1724 by Daniel Gabriel Fahrenheit and it is still a subject of deep research [8]. Dorsey published one of the early comprehensively studied cases of the freezing of supercooled water. He reported that water can be supercooled until -20 °C using ordinary freezing methods and explored various parameters that can influence the supercooling of water such as

effect of preheating, filtration, duration of cooling, rate of nucleation, mechanical initiation of freezing, etc. [6]. Wilson provided further clarification about the freezing phenomenon that occurs after supercooling wherein the freezing action was classified into homogenous and heterogenous nucleation. Homogenous nucleation occurs when there are no impurities in the water sample and the homogeneous nucleation temperature was proposed to be approximately around -39 °C [7]. Heterogenous nucleation is even more difficult to predict as the temperature in which nucleation occurs is dependent on the number of impurities or solutes in the water sample which can act as nucleation sites. Homogenous nucleation is very difficult to achieve in a practical setting, even in laboratory conditions. As such, except for ultra-pure water insulated in emulsions that can eliminate contact with solid surfaces, all other aqueous solutions are said to undergo heterogeneous nucleation [7]. Due to the impractical nature of achieving homogenous nucleation and the variable nature of heterogeneous nucleation, the current experiment takes a practical approach of studying normal tap water due to the ease of access and practical usage in the industry.

1.3. Ultrasonics

Ultrasonics is the science and application of ultrasound waves. All acoustic sound waves that have frequencies greater than 20 kHz are considered as ultrasonic waves and are inaudible to the human ear. Ultrasonics can be categorized into 2 types [9]:

1. Low-Intensity Applications
2. High-Intensity Applications

Low-intensity ultrasonics deals with those ultrasonic applications that require low power input (on the order of milliwatts) and operate at high frequencies (on megahertz

scale). Some applications of low-intensity ultrasonics are non-destructive testing methods, intrusion detection, measurement of elastic properties, medical diagnosis, delay lines, and signal processing [9]. High-intensity ultrasonics deals with those ultrasonic applications that require a large magnitude of power input (on the order of 10 W to several 1000 W depending on the application) and operate over a low frequency range (between 20 kHz to 100 kHz). High-intensity ultrasonics is sometimes referred to as "Power Ultrasonics" when working with power levels equal to or greater than 10 W. Some applications of high-intensity ultrasonics are ultrasonic cleaning, welding plastics, machining, soldering and sonochemistry [9]. As the current study focuses on high-intensity ultrasound, this category is discussed in further detail.

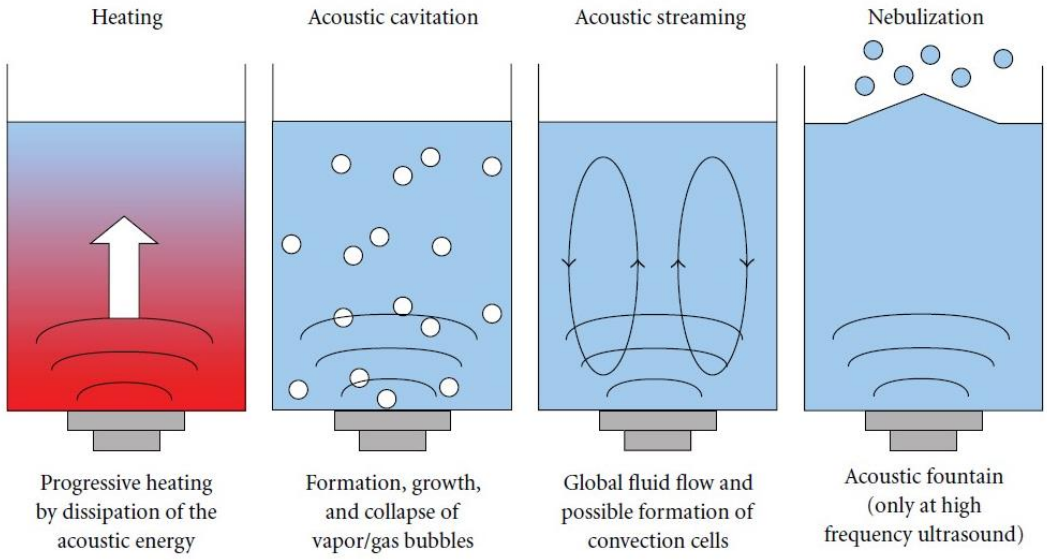

Figure 1.2: Ultrasound induced effects in a liquid.[10]

Legay et al. conducted a review on the topic of application of power ultrasound in a liquid medium which results in several microscale phenomena such as heating, cavitation, streaming and nebulization as shown in Figure 1.2 that can help in heat transfer enhancement. Among these effects, acoustic cavitation and acoustic streaming

are the two important factors that are mainly attributed to the heat transfer enhancement in fluids. Acoustic streaming is defined as the formation of jets and circulation pathways due to the absorption of high-amplitude propagating ultrasonic waves inside a liquid medium [11]. It is reported that the circulation and fluid movement provided by this phenomenon induces greater heat convection and turbulence in the medium, thereby enhancing the heat transfer rate [10]. Acoustic cavitation is defined as the generation, expansion, oscillation, and collapse of bubbles inside a liquid medium in a time-varying acoustic field. When the local pressure is reduced below the vapor pressure under ultrasonic conditions (when gas dissolution is present), the static pressure and the cohesive forces are overcome to form gas bubbles which oscillate and collapse violently [10]. This collapse results in a sudden local pressure increase up to 193 MPa [12]. The resulting bubble implosion causes disturbances to the thermal boundary layer which results in a reduction of thermal resistance and heat transfer improvement.

1.4. Effect of Ultrasound on Supercooling and Freezing Processes

Several researchers have reported using ultrasound as a potential method to overcome supercooling and improve the heat transfer in the freezing process of water to ice [13]–[20]. Dalvi-Isfahan et al. published a review on the control of ice nucleation by ultrasound, electric and magnetic fields and reported that the effects of electric and magnetic fields in some cases are said to be contradictory and less effective when compared to the effects of ultrasound on the control of nucleation, which indicates that further research into mechanisms of these processes is required. It was also stated that it was necessary to test the scalability of these technologies and that further

optimization was required to make them applicable for industrial settings [13]. Inada et al. reported that when ultrasonic vibration was applied at 28 kHz and tested between 0-100W, freezing was successfully initiated in both tap water and pure water. This was attributed to the ultrasonic cavitation phenomenon which helped create nucleation sites and that the freezing temperature can be controlled by controlling the cavitation intensity [15]. Zhang et al. utilized ultrasound at 39 kHz and an ultrasonic intensity of 4.4 kW/m^2 to further investigate the generation of ice slurries from supercooled water as well as the effect of bubble nuclei.

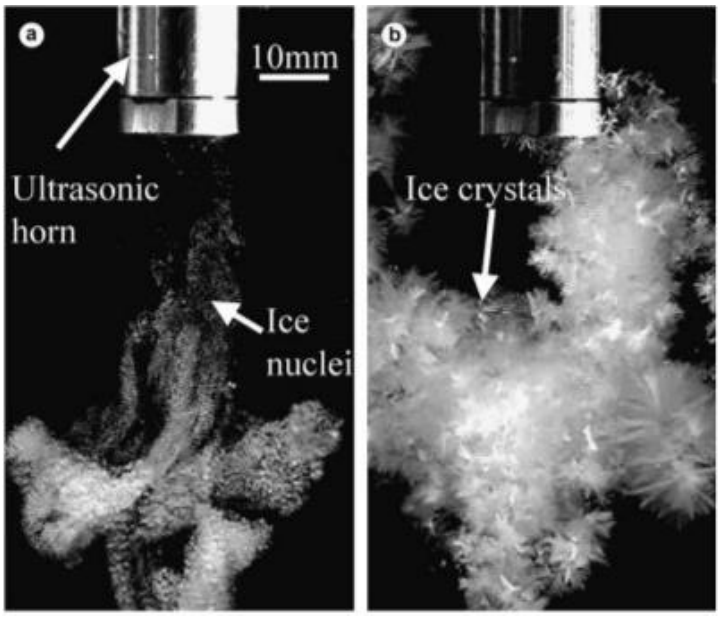

Figure 1.3: Ice crystals nucleated by an ultrasonic device (a) ice crystal following an ultrasonic pulse, (b) crystals 5 s later. [19]

It was reported that a high density of fine ice crystals was observed at the onset of ultrasound as seen in Figure 1.3 and the effect of ultrasound improves with an increase in the number of bubble nuclei sites [16]. Hozumi et al. reported that ultrasound applied at 45 kHz with an intensity of 0.13 W/cm^2 & 0.26 W/cm^2 helped in initiating nucleation. It was also reported that the nucleation effect increased with ultrasonic power and that

the cavitation phenomenon was absent with reduced power [17]. Chow et al. studied the effect of a primary and secondary pulse of ultrasound at 20 kHz on supercooled water. The effect of the primary pulse reaffirmed the previous observation about increased ultrasonic power providing greater nucleation effects. It was reported that the effect of the secondary pulse led to fragmentation of pre-formed ice crystals and that there were flow patterns observed around cavitation bubbles which could have also contributed to the fragmentation. Figure 1.4 provides a pictorial explanation of the effect of ultrasound on ice crystal structures [19].

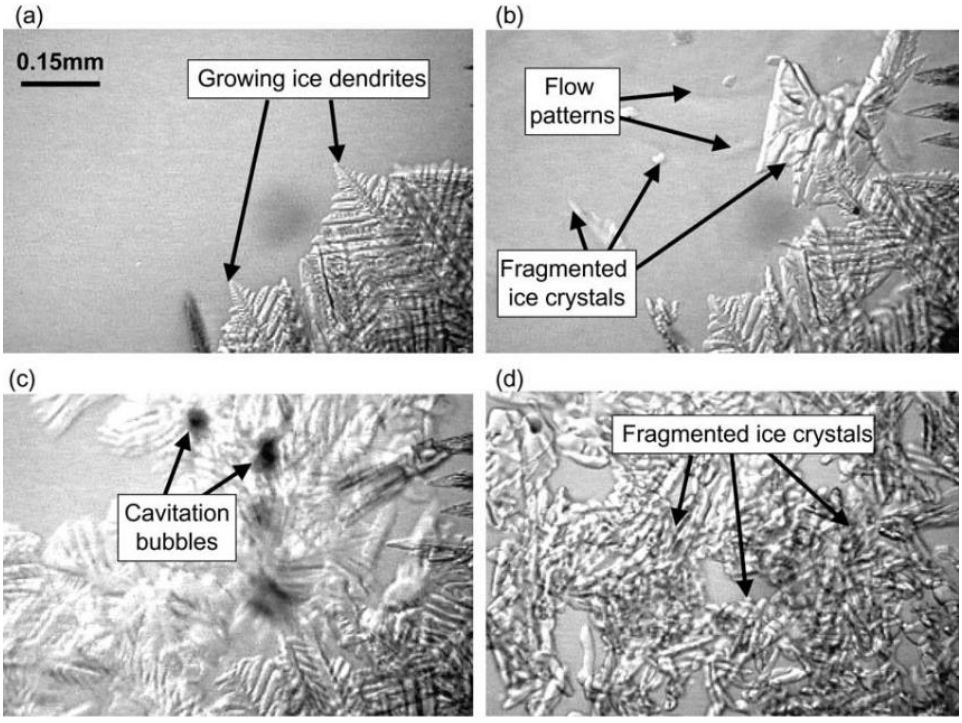

Figure 1.4: Microscopic effect of ultrasound on the secondary nucleation of ice in a 15 wt.% sucrose solution. (a) crystal before ultrasound (b)(c)(d) crystal structure after ultrasonic application [21]

1.5. Effect of Ultrasound on the Supercooling of PCMs

Water is used as a thermal latent energy storage medium in several disciplines and is studied as a Phase Change Material (PCM), wherein supercooling is found to be a undesirable component [18]-[19]. Cui et al. and Jia et al. studied the combined effect of nanoparticles and ultrasound on the supercooling of water and found that the supercooling degree decreases with an increase in ultrasonic intensity and nanoparticle concentration. But the reduction of supercooling degree caused by ultrasound and nanoparticles together do not exceed the sum of the supercooling degree reductions caused by ultrasound and nanoparticles separately [20]- [21]. Liu et al. investigated the effects of graphene oxide nanosheets and ultrasound on the supercooling and nucleation behavior of nanofluids PCMs and reported similar results of reducing nucleation time of the phase change process [26]. Yan et al. investigated the effect of ultrasound on the melting phase change process of paraffin PCM and reported that the effect of ultrasound drastically increased the heat transfer properties and the phase change rate [27]. This provides further indication that ultrasound has a positive effect on phase change processes both in terms of solidification as well as melting.

1.6. Effect of Ultrasound on Food Freezing Applications

Application of ultrasound on food freezing technologies is a prevalent topic in recent times. Review articles have been published regarding the effect of ultrasound during food freezing processes wherein various food types were analyzed and discussed in terms of freezing behavior under ultrasonic application. It was established that ultrasound helps in increasing the freezing rate of the products and controlling the size and distribution of ice crystals which led to an overall increase in the quality of products. Other applications such as low-intensity diagnostic ultrasound was used to

monitor the crystal structure and freezing rate. It was reported that the effects of ultrasound on the freezing processes were attributed to cavitation and microstreaming phenomena which helped in the nucleation and heat transfer enhancement, respectively [28], [29].

It is understood that supercooling prolongs the freezing time which can potentially cause unnecessary energy consumption. Although past research has provided very useful insights on the ultrasound-induced microscale phenomena related to freezing processes, there is a lack of research from an energy consumption standpoint. Given that the application of ultrasound is an energy intensive process, and that ultrasonic energy is heat dissipating in nature, it becomes necessary to properly optimize the application of ultrasound when conducting experiments to ensure additional energy is not wasted and more so does not negatively affect the freezing process. Therefore, the current experiment aims to establish the extent of supercooling overcome by ultrasound, its effect on the overall freezing process and finally analyze various parameters such as ultrasonic power, frequency/time of application of ultrasound (not to be confused with ultrasonic frequency) and duration of application.

CHAPTER 2

EXPERIMENTAL PREPARATION

The current research is designed to observe the supercooling phenomenon of water and conduct a comparative study on the effect of ultrasound on supercooling for varying parameters by recording the overall energy consumption across the various iterations of the experiments. The literature review conducted prior to the experiment helped provide the necessary insight needed to design and fabricate the cooling module, prepare the ultrasonic transducer as well as the temperature measuring instruments required for the experiment. The experimental set-up was designed with the objective of measuring temperature readings at various locations inside the water domain and to measure the inlet and outlet temperatures of the coolant used in the freezing process. The following section discusses the various components and procedures that were utilized during the experiment.

2.1. Cooling Module Design

The cooling module consists of the aluminum container, copper cooling blocks and thermocouples as shown in Figure 2.1. The dimensions of the aluminum container are 9.1 cm × 3.9 cm × 4.9 cm with a thickness of 0.3 cm. The material used for the container is aluminum 6061 alloy. The cooling blocks were made from pure copper for their excellent thermal properties and uniform surface temperature characteristics. The dimensions of the cooling block are 4 cm × 4 cm × 0.9 cm. 4 K-Type thermocouples were placed inside the aluminum container at specific locations and have a wire diameter of 0.48 mm. They are referred to as Reference thermocouple, X-direction thermocouple, Y-direction thermocouple, and Z-direction thermocouple. These 4

thermocouples are utilized to properly capture the temperature variations across the cooling container during the freezing process. The thermocouples X,Y and Z are specifically placed at locations to produce temperature gradients with respect to the Reference thermocouple.

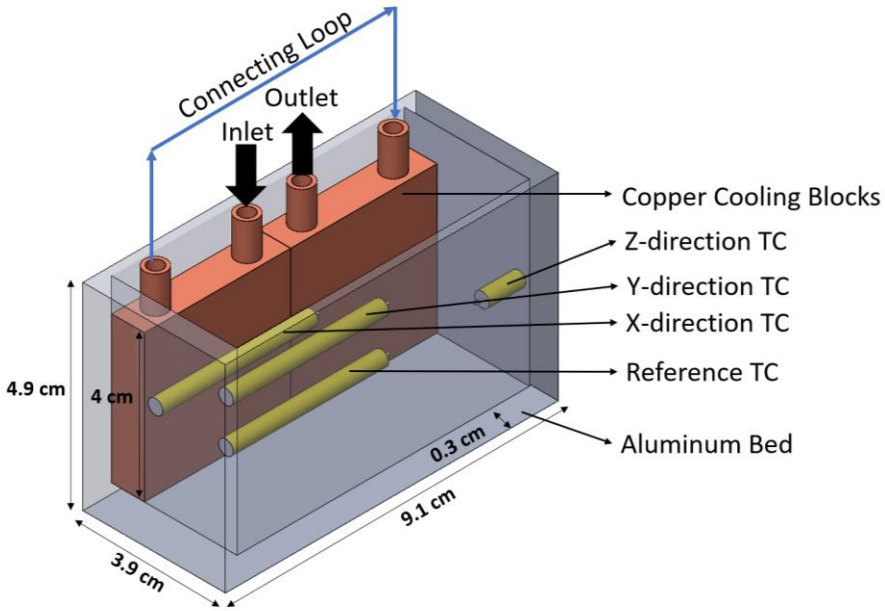

Figure 2.1: CAD design of the cooling module

The Reference thermocouple has a length of 2.45 cm and is placed at a height of 4.25 cm and 0.3 cm away from the wall opposite to the copper blocks. The Reference thermocouple is placed at a middle level on the opposite side of the copper cooling blocks. The X-direction thermocouple is placed at the same height and length of Reference thermocouple, but the width is adjusted to 0.2 mm closer to the copper blocks to monitor the temperature of cooling blocks. The Z-direction thermocouple is placed at the same horizontal plane as the Reference thermocouple, but the length is reduced to 0.3 cm from the left side of the container. The Y-direction thermocouple is placed 1.2 cm above the Reference thermocouple to measure the vertical temperature

variations as well as to measure the temperature of the water close to the surface that is open to the atmosphere. A volume of 76 ml of water is used to test the freezing process inside the cooling module, wherein the Y-thermocouple is positioned right below the top surface of the water.

2.2. Components of the Experiment

The current section presents the various components and materials used for the construction of this experimental set-up. Table 2.1 presents the instruments and components used in the current experiment.

Table 2.1: Components used in the experimental set-up.

Component	**Manufacturer**	**Model**	**Quantity**
Polystat® Thermal Bath	Cole-Parmer	BOM:2123338000	1
Ultrasonic Transducer	Beijing Ultrasonics	28 kHz	1
Thermocouples	Omega Instruments	K-Type	7
Copper Block	Kalolary	-	2
DAQ Board	National Instruments	NI 9212	1
Flowmeter	Omega Digital Flowmeter	FLR1011 Serial no: 12064	1
Pump	Micropump	GJ-N21.JF1ZSA	1
Function generator	Siglent Technologies	SDG1032X	1
Amplifier	AALABSYSTEMS	A-303	1
Reference Thermocouple	Thomas Scientific	1227U09	1
Ethylene Glycol solution (Coolant)	Shop Pro	50% Glycol – 50% Water	7.56 L
Silicone Glue	GE	Advanced Silicone	-
Epoxy	JB Weld	-	-
Insulation	Armacell	AP/Armaflex	0.3cm thickness
Computer	-	LabVIEW software	1
Tap water	-	-	76 ml

2.3. Experimental Set-up

After the initial design of the cooling module was determined, the cooling module was fabricated using Aluminum 6061 alloy as the base material for the cooling module container and well sealed using epoxy resin to prevent any leakage. Copper cooling blocks were purchased and used as the heat transfer instruments for their exceptional thermal properties. Tap water was studied in this experiment wherein 76 ml of water was used in all the experiments. A preliminary experiment was conducted using a single copper cooling block which resulted in a weak heat transfer rate and low ΔT (temperature difference) between the inlet and outlet temperatures of the coolant which drastically affected the uncertainty of the experiment. Therefore, to improve the uncertainty of the experiment, 2 copper blocks were placed in series to ensure better heat transfer rate. The copper cooling blocks were attached to the side of the container using silicone glue. Holes were drilled into the sides of the cooling container at appropriate locations to accommodate the thermocouples. The thermocouples utilized in the experiment were fabricated in the lab using thermocouple wires, super glue, and wire cutters. After stripping the thermocouple wires into positive and negative junctions at both ends, one end was used to measure the temperature. The electrical contact is maintained between the two thermocouple wire tips by tightly winding them together using a needle nose plier. The exposed wire portion below the tip was sealed with super glue to prevent water from passing through the insulation of the thermocouple which can cause errors in the temperature readings. The wire tips were not soldered together to avoid additional metallic contacts that can affect the system.

The thermocouple wires were then cut according to the appropriate dimensions and then placed inside the container through the drilled holes as specified in Figure 2.1.

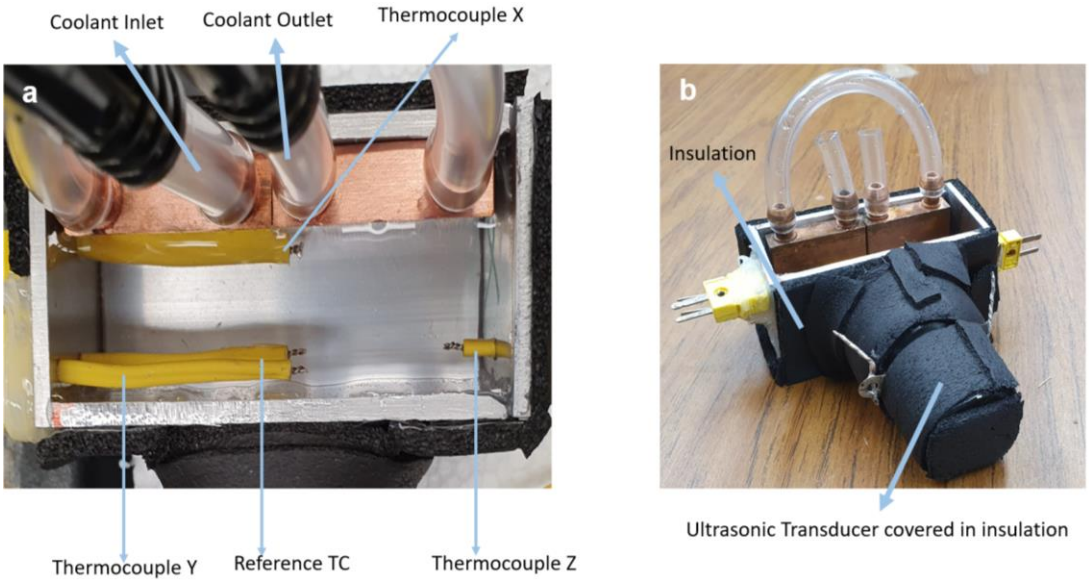

Figure 2.2: Experimental prototype of the cooling module (a) Top view (b) Isometric view.

Figure 2.2 shows the experimental set-up of the cooling module. After the thermocouples are placed into the cooling container, they are sealed using silicone glue on the outer surface of the container to prevent any leakage of water. The ultrasonic transducer shown in Figure 2.3 is attached to the side of the aluminum container opposite to the copper cooling blocks using a thin layer of epoxy which helps to tightly hold the transducer onto the aluminum container surface. A very close contact between the transducer surface and container surface is maintained for the proper transmission of ultrasonic energy.

Figure 2.3: Ultrasonic transducer

The insulation material was then applied to the exposed outer surfaces of the aluminum container and transducer to minimize heat gains from the external atmosphere during the cooling process. The R-value for the insulation tape was 0.5 $m^2 K\ W^{-1}$ as provided by its specifications [30]. After the cooling module was readied, the appropriate coolant fluid was prepared for the experiment. To ensure a safe experiment that would not damage the equipment, it was decided that a coolant temperature of -10 °C would be appropriate. Therefore, a solution of ethylene glycol and water at 50% was used as a coolant for the experiment. A total of 7.56L of the solution was prepared and stored inside the thermal bath. The thermal bath used in this experiment is the Polystat® Thermal Bath manufactured by Cole-Parmer as shown in Figure 2.4 which has a capacity of 15L. This thermal bath has a temperature range of -40 °C to 200 °C.

Figure 2.4: Thermal bath

The coolant used as the heat transfer medium is diluted ethylene glycol solution (Ethylene Glycol 50% - Water 50%). The glycol coolant is circulated through the cooling blocks for the heat transfer application. Throughout the experiment, the temperature of the coolant varies between ± 0.9 °C. Therefore, the properties of 50% diluted ethylene glycol solution at -10 °C were used which were obtained from industrial data sheets provided by Dow chemicals as shown below in Table 2.2 [31].

Table 2.2: Properties of 50% diluted ethylene glycol solution at -10 °C

Material Property	**Amount**	**Units**
Density	1085.4	$\frac{kg}{m^3}$
Dynamic Viscosity	0.01274	$Pa.s$

Specific Heat	3.166	$\frac{kJ}{kg\ .\ K}$
Thermal Conductivity	0.344	$\frac{W}{m\ .\ K}$

The coolant inlet and outlet temperatures need to be measured to calculate the energy flowing into and out of the system. A differential thermocouple was made in the lab using K-Type thermocouple wires to measure the ΔT temperature difference of the coolant flowing through the inlet and outlet locations. A tee plastic connector was fashioned to place the thermocouple tips inside the flowing coolant at both locations as shown in Figure 2.5. The thermocouple wires are fastened inside the tee connector using epoxy resin and silicone glue to ensure that the wires are properly fixed and sealed in position as they are easily prone to leakage.

Figure 2.5: Tee pipe connector

The working principle of a thermocouple was described by Thomas Seebeck in 1821 when he discovered that the voltage generated by a conductor is proportional to a temperature difference [32]. When two dissimilar conductors of varying electrical properties are

connected, a temperature difference at different ends produces a voltage difference known as the thermoelectric or Seebeck effect which is expressed as

$$V = S\Delta T \tag{2.1}$$

where S is the Seebeck coefficient (V/K) dependent on the material property of the connecting wires used for the temperature measurement. Generally, individual thermocouples are used in a temperature difference measurement, but this causes greater uncertainty in the result. The combined limit of error in the ΔT is found by taking the square root of the sum of the squares of the limits of error (U_{T1} & U_{T2}) corresponding to the uncertainty error associated with the individual thermocouples:

$$U_{\Delta T} = \sqrt{{U_{T1}}^2 + {U_{T2}}^2} = \sqrt{2}\, U_{\Delta T} \tag{2.2}$$

The coefficient $\sqrt{2}$ of $U_{\Delta T}$ in the above equation can be eliminated when a differential thermocouple is employed. The differential thermocouple is configured as shown in Figure 2.6.

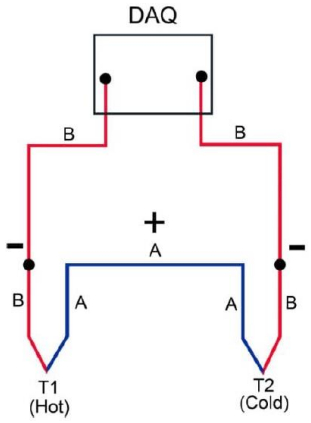

Figure 2.6: Differential thermocouple configuration[33]

The K-Type thermocouples were purchased from Omega Instruments and have a wire diameter of 0.48 mm. They are rated with a sensitivity of approximately 41 μV/°C [34]. They are inexpensive and have a wide operating temperature range between −200 °C to 1350 °C. All the thermocouples were calibrated using a Thomas Scientific reference thermometer which is certified as per NIST standards with the certification number of 4244-11552989. The thermometer measurements were certified to be accurate at the specific temperatures of 0 °C, 25 °C & 37 °C up to an accuracy of ±0.01 °C. Measurements at all other temperatures are ascribed with an accuracy of ±0.05 °C. Therefore, after proper calibration of the thermocouples using the temperature bath and reference thermometer, an uncertainty of ±0.05 °C is assigned to the thermocouples. The cold junction compensation for the thermocouples is calculated and corrected using the built-in sensor within the NI Data Acquisition Board (DAQ) 9212 which has a reported accuracy of 0.01 °C. The flow rate for the experiment was measured using an Omega Digital Flowmeter and was determined to be 0.004301 kg/s with uncertainty of ±1%. The pump used for the experiment was manufactured by Micropumps and has a working temperature range of −46 °C to 121 °C. An extra thermocouple is placed at the outer surface of the insulation material to measure the surface temperature of the insulation which is used to calculate the insulation heat gains.

2.4. Measuring the Resonant Frequency of the Ultrasonic Transducer

It is necessary to measure the power input into the piezoelectric transducer during the experiment and use the appropriate resonant frequency of the transducer when coupled with the cooling module. The resonant frequency of an ultrasonic transducer depends upon

its material composition, geometry orientation, and the subject to which the transducer is coupled. Resonance frequencies of a transducer change depending on its un-coupled (unattached) and coupled states. Manufacturers provide a value for the natural resonance frequency of a transducer element, but this value corresponds to the uncoupled condition. When the resonant frequency is not achieved during application, it can greatly affect the electrical and mechanical efficiency of the sonication process. The transducer used for the experiment is 28 kHz in an unloaded condition as specified by the manufacturer. Once coupled to the cooling module, the natural frequency needs to be determined.

The power supplied to the transducer can be expressed in terms of AC power input using Ohm's law for AC current:

$$V_m \sin(\omega t) = Z * I_m \sin(\omega t - \varphi) \tag{2.3}$$

where V_m is the average voltage, I_m the average current, Z the impedance, ω frequency, t time, and φ the phase angle between the voltage and current. At the natural resonant frequency of the piezoelectric element, the impedance to the transducer is at its lowest which allows the transducer to draw maximum power and ensures that the highest amount of electrical power is converted into mechanical vibrations. An oscilloscope, a function generator and shunt resistor are used as shown in the circuit diagram in Figure 2.7 to vary the frequencies and calculate the impedance to the transducer by measuring the current and voltage values obtained from the oscilloscope. Therefore, the natural frequency of the transducer was determined to be 26.13 kHz which is the natural frequency of the coupled system.

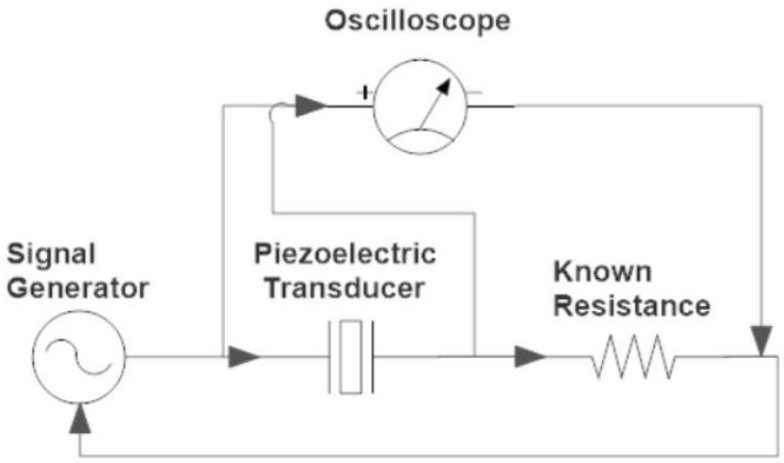

Figure 2.7: Circuit to measure the resonant frequency of the piezoelectric element [35]

2.5. Experimental Procedure

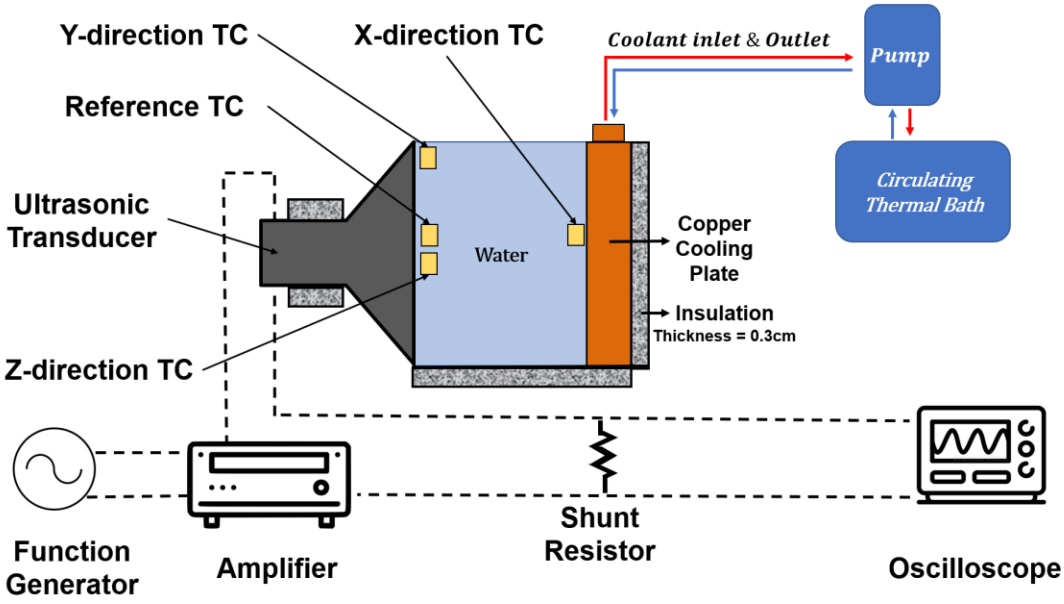

Figure 2.8: Schematic diagram of the experiment

Figure 2.8 shows the schematic diagram for the experiment. Once all the appropriate connections are made, the circulating temperature bath is turned on and a coolant

temperature of −10 °C is attained. Tap water is measured up to 76 ml using a beaker and poured into the cooling container. The thermocouples are connected to the DAQ module and the initial temperatures inside the container are measured. The temperature data are recorded every 1 second using LabVIEW software connected the DAQ module. Once the temperatures inside the container are stabilized, the experiment is ready to begin. The experiments are conducted as non-ultrasonic and ultrasonic experiments. The non-ultrasonic experiments are conducted to observe the period and degree of supercooling as well as to measure the energy consumption in the overall freezing process of water. The ultrasonic experiments are conducted to observe the extent of reduction in supercooling when ultrasound is applied. The ultrasonication is applied immediately after any one of the thermocouple temperature readings reach 0 °C and the sonication is stopped when the last thermocouple reading dips below 0 °C. This procedure is devised to ensure that ultrasound is only applied during the phase change process of water wherein the temperature of the water stagnates at 0 °C. Once the last thermocouple reading drops below 0 °C, the application of ultrasound is stopped, and the freezing process is continued until all the readings reach a temperature of −2 °C after which the experiment is stopped and the energy consumption for the entire process is calculated including the power supplied for the ultrasonication. The surfaces of the aluminum container and the copper blocks were cleaned using diluted vinegar at certain points between experiments to remove any scaling contaminants and oxidation on the copper surface that can affect the experiment. The oscilloscope, generator and amplifiers are utilized to control the piezoelectric transducer when the ultrasonic experiments are conducted. Figure 2.9 shows a complete set-up of the experiment.

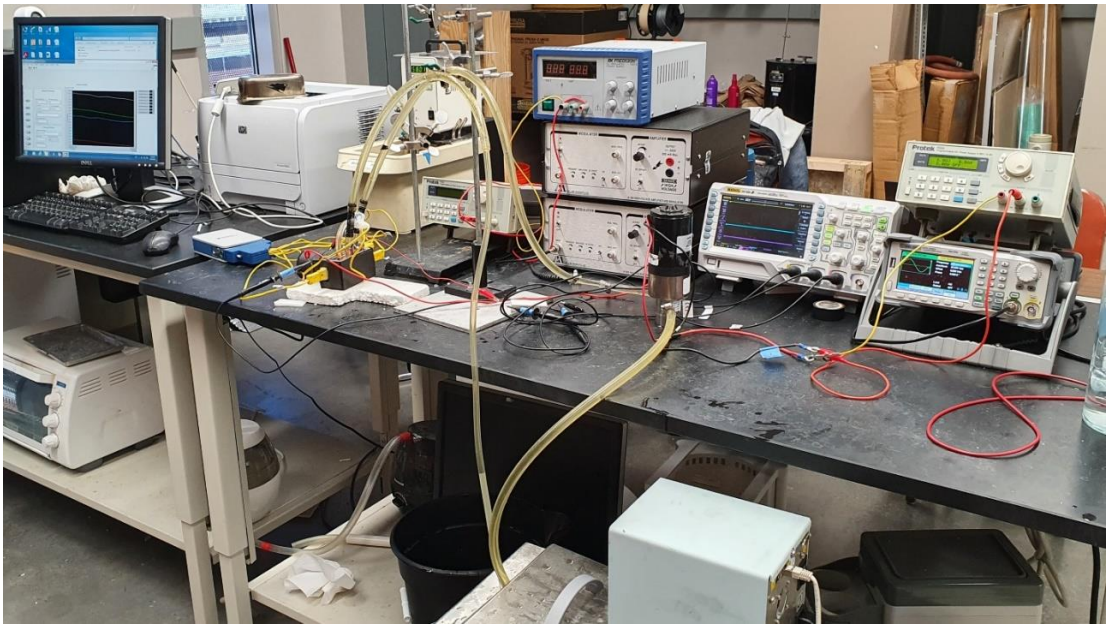

Figure 2.9: Experimental set-up

CHAPTER 3

METHODOLOGY

3.1. Theory

This section discusses theory, formulae and approaches used for the analysis of the experiments.

The instantaneous power input into the system is calculated using:

$$\dot{E} = \dot{m} \times C_p \times (T_{out} - T_{in}) = \dot{m} \times C_p \times \Delta T \qquad (3.1)$$

where $\dot{E}$ is the instantaneous cooling power supplied for the freezing process, $\dot{m}$ the flow rate of the coolant, C_p the specific heat capacity of the coolant and ΔT the temperature difference between the inlet and outlet temperatures.

The power supplied to the ultrasonic transducer must also be accounted for. The ultrasonic power was determined using:

$$P_{US} = V_{rms} \times I_{rms} \times cos\theta \qquad (3.2)$$

where V_{rms} is the root mean square value of voltage across the transducer, I_{rms} the root mean square value of alternating current passing through the transducer, and θ the phase angle between the voltage and current.

The heat transfer through the insulation is calculated as given below:

The heat gain from the vertical sides of the aluminum container is calculated by measuring the temperature of the insulation outer surface and calculating the heat gain via natural convection. The equations for natural convection heat and mass transfer are obtained from [36]. For all the calculations, the ambient temperature was measured to be 24 °C.

Firstly, the Rayleigh number, Ra_L is calculated from:

$$Ra_L = \frac{g\beta(T_s - T_\infty){L_c}^3}{\nu^2} \times Pr \tag{3.3}$$

where g is the gravity constant, β the thermal expansion coefficient, T_s the surface temperature, T_∞ the temperature far away from the surface, L_c the characteristic length, ν the kinematic viscosity and Pr the Prandtl number.

The Nusselt number calculation, Nu, is done based on the calculated Rayleigh number:

$10^4 < Ra < 10^9$ $$Nu = 0.59\ {Ra_L}^{1/4} \tag{3.4}$$

$10^{10} < Ra < 13$ $$Nu = 0.1\ {Ra_L}^{1/3} \tag{3.5}$$

The thermal properties of air are obtained at the film temperature $T_f = (T_s + T_\infty)/2$, which is used for the calculations. After the Nusselt number is calculated, it is used to find the natural convection heat transfer coefficient, h_{conv}, and the heat gain, Q, for the vertical sides at the outer surface of the insulation material:

$$h_{conv} = \frac{k\ \times Nu}{L} \tag{3.6}$$

$$Q = h \times A \times (T_s - T_\infty) \tag{3.7}$$

Since the transducer is in contact with the aluminum container, it is also covered with insulation to prevent heat gains into the system. The transducer is considered as a horizontal cylinder undergoing natural convection heat gains. The previous steps done for the natural convection calculation for a vertical plate are repeated with modified equations with respect to a horizontal cylinder as given by equations 3.8 to 3.11:

$$Ra = \frac{g\beta(T_s - T_\infty)D^3}{\nu^2} \times Pr \tag{3.8}$$

$$Nu = \left\{ 0.6 + \frac{0.387\, Ra_D{}^{1/6}}{\left[1 + (\frac{0.559}{Pr})^{9/16}\right]^{8/27}} \right\}^2 \quad (3.9)$$

$$h_{conv} = \frac{k \times Nu}{D} \quad (3.10)$$

$$Q = h \times A \times (T_s - T_\infty) \quad (3.11)$$

where D is the diameter of the horizontal cylinder.

Simultaneous heat and mass transfer calculations from the top surface of the water:

The current set-up is an open system where the top surface is open to the atmosphere. This is done to observe the formation of ice crystals during the freezing process. It should also be noted that a cause for concern might be argued in terms of heat gain from the atmosphere into the system. As this is a comparative study between varying parameters where the external atmospheric conditions are kept constant, the uniformity of the experiments compensates for any additional heat gains and energy wastages. But for the analysis, the heat gains from the external environment are calculated. The Y-Thermocouple is assumed to measure the temperature of the top surface as it is placed as closely as possible to the surface. Since most of the experiment deals with the phase change process of water at 0℃, the surface temperature calculations are conducted for $T_s = 0$ °C. The humidity inside the laboratory environment was assumed to be $\emptyset = 40\%$.

The properties of water at 0 °C and the properties of air at 24 °C are obtained. The air–water vapor mixture is dilute and thus dry air properties for the mixture at the average temperature of $(T_s + T_\infty)/2$ are used. The equations for the simultaneous heat and mass

transfer calculations are obtained from [36]. The vapor pressure of air, $P_{v,\infty}$, far from the water surface is calculated based on the relative humidity and vapor saturation pressure at 24 °C, $P_{sat,\infty}$:

$$P_{v,\infty} = P_{sat,\infty} \times \emptyset \tag{3.12}$$

The water vapor and the air are treated as ideal gases and the total atmospheric pressure is the sum of the vapor and dry air pressures. Therefore, the densities of the water vapor, dry air, and their mixture at the water–air interface and far from the surface are determined using equations 3.13 to 3.18:

At the surface:

$$\rho_{v,surface} = \frac{P_{v,surface}}{R_v T_s} \tag{3.13}$$

$$\rho_{a,surf} = \frac{P_{a,surface}}{R_a T_s} \tag{3.14}$$

$$\rho_{surface} = \rho_{a,surface} + \rho_{v,surface} \tag{3.15}$$

Away from the surface:

$$\rho_{v,\infty} = \frac{P_{v,\infty}}{R_v T_\infty} \tag{3.16}$$

$$\rho_{a,\infty} = \frac{P_{a,\infty}}{R_a T_\infty} \tag{3.17}$$

$$\rho_{\infty} = \rho_{v,\infty} + \rho_{a,\infty} \tag{3.18}$$

The characteristic length, L_c, is calculated below, where A_s is the surface area and P is the perimeter:

$$L_c = \frac{A_s}{P} \tag{3.19}$$

Densities of the mixture are used instead of temperatures for the Grashof number calculation due to the non-homogenous mixture:

$$Gr = \frac{g(\rho_{surface} - \rho_{\infty}){L_c}^3}{\rho\nu^2} \tag{3.20}$$

Considering the case for a natural convection heat transfer for a horizontal surface (upper surface of a cold plate), the following calculations are done:

$$Nu = 0.27\ (GrPr)^{1/4} \tag{3.21}$$

$$h_{conv} = \frac{Nu\ \times k}{L_c} \tag{3.22}$$

$$Q_{conv} = \ h_{conv}\ \times A_s \times (T_s - T_{\infty}) \tag{3.23}$$

The mass diffusion is also considered for the top surface of the water. The diffusion coefficient, D_{H_2O-Air}, is calculated as follows, where T is the average temperature between the surface and ambient temperature and P_{atm} is the atmospheric pressure:

$$D_{H_2O-Air} = 1.87 \times 10^{-10} \times \frac{T^{2.072}}{P_{atm}} \quad (3.24)$$

The Schmidt number Sc, Sherwood number Sh and Mass transfer coefficient h_{mass} formulae are shown in equation 3.25 to 3.27:

$$Sc = \frac{\nu}{D_{AB}} \quad (3.25)$$

$$Sh = 0.27\ (Gr \times Sc)^{1/4} \quad (3.26)$$

$$h_{mass} = \frac{Sh \times D_{AB}}{L_c} \quad (3.27)$$

The rate of mass diffusion, m_v, is calculated below:

$$m_v = h_{mass} \times A_s \times (\rho_{v,\infty} - \rho_{v,s}) \quad (3.28)$$

Heat transfer due to mass diffusion, Q_m, is calculated from:

$$Q_m = m_v \times h_{fg} \quad (3.29)$$

Thermal Mass calculation:

The thermal mass of the cooling module, $Q_{thermal\ mass}$, is calculated for the total temperature range of the experiment:

$$Q_{thermal\ mass} = m \times C_p \times \Delta T \qquad (3.30)$$

Total Energy Calculation:

The total energy consumed for a given experiment is calculated using the following equation:

$$E = \sum \dot{E} \times \Delta t \qquad (3.31)$$

where $\dot{E}$ is the instantaneous power supplied for the cooling load calculated using equation 3.1 and Δt is the time period associated with the instantaneous power supplied which is 1 second corresponding to the sampling rate of the DAQ.

3.2. Uncertainty Analysis

It is important to calculate the uncertainty of the various measured parameters in an experimental study. The calculated uncertainty for a result reveals the level of confidence ascertained to the conclusions of any experiment. Therefore, uncertainties in an experiment should be maintained at a low level. Uncertainty is categorized into bias and precision components which are discussed below. The following equations are obtained from [37].

For a given experimental result, *y*, which is a function of *n* number of variables *x*,

$$\mathrm{y} = \mathrm{f}(x_1, x_2, \ldots, x_n)$$

the general case for the bias uncertainty (U_y) in the experimental results can be given by

$$U_y = \sqrt{\left(\frac{\partial y}{\partial x_1} U_{x_1}\right)^2 + \left(\frac{\partial y}{\partial x_2} U_{x_2}\right)^2 + \left(\frac{\partial y}{\partial x_3} U_{x_3}\right)^2 + \cdots + \left(\frac{\partial y}{\partial x_n} U_{x_n}\right)^2} \qquad (3.32)$$

where U_{x1},U_{x2} ,U_{x3}...U_{xn} are the uncertainties in the primary measurements.

Therefore, the bias uncertainty equation for the cooling energy input is calculated using equation 3.33:

$$U_{E_{bias}} = \sqrt{\left(\frac{\partial E}{\partial \dot{m}} U_{\dot{m}}\right)^2 + \left(\frac{\partial E}{\partial \Delta T} U_{\Delta T}\right)^2} \tag{3.33}$$

The specific heat capacity, C_p, is assumed as a constant value of 3166 J kg^{-1} K^{-1}for the calculations due to the minimal changes in the temperature difference that do not drastically affect the heat capacity value.

The accuracies of the individual measurements in the cooling energy are shown in Table 3.1.

Table 3.1: Uncertainties of measured parameters

Parameters	**Uncertainty**	**Units**
$\dot{m}$	$\pm$1%	kg/s
ΔT	$\pm$0.05	K
V_{rms}	$\pm$0.2%	V
I_{rms}	$\pm$0.2%	A

Therefore, the maximum bias uncertainty in the cooling energy input E is calculated to be $\pm$4.3%.

The individual contributors to the uncertainty in the ultrasonic power input are V_{rms} & I_{rms}, each accounting for $\pm$0.2% uncertainty, respectively. Equation 3.34 gives the bias uncertainty associated with supplied ultrasonic power:

$$U_{P_{US_{bias}}} = \sqrt{\left(\frac{\partial P_{US_{bias}}}{\partial V_{rms}} U_{V_{rms}}\right)^2 + \left(\frac{\partial P_{US_{bias}}}{\partial I_{rms}} U_{I_{rms}}\right)^2} \tag{3.34}$$

The phase angle $cos\theta$ is considered as a constant of 1 in the above equation. Using equation 3.34, the bias uncertainties for 10W and 3.5W of ultrasound were calculated as ±0.3% and ±0.3% respectively. As the power supplied to the transducer remains constant, there is no precision uncertainty associated with the ultrasonic power. As such, when comparing the total uncertainty of the ultrasonic power with the uncertainty of the energy input, it is much lower by several magnitudes. Therefore, the uncertainty due to the ultrasonic power is negligible.

Precision uncertainty (or random error) pertains to various uncontrollable factors such as the environmental conditions and human errors present during an experimental run. Therefore, this error focuses on the errors produced across various repetitions of the experiment and recording the inconsistencies for a set of experiments. In the current study, precision uncertainty is highly significant due to the unpredictable nature of the experiment attributed to the occurring supercooling effect. Therefore, it becomes necessary to record and calculate the precision uncertainty for the measured parameters.

Table 3.2: Energy consumption for the repeated non-ultrasound experiments

Experimental Run	**Total Energy (J)**
#1	25057.4
#2	19958.1
#3	22763.2
#4	34702.8
#5	30415.6
#6	26902.9
#7	29079.2
#8	29825.4
#9	30821.8
#10	27670.4

#11	31577.0
#12	28613.3
#13	32808.6
#14	29385.4
#15	31328.1
#16	28989.6
#17	32980.9

Table 3.2 provides the data on the repeated results of the non-ultrasonic supercooling experiments of water. The precision error is calculated using a Student's t-method [37] to find the confidence interval for the given set of data. The Student's t-distribution method is useful for determining the confidence intervals up to 95% for data sets less than 30 samples, which means that 95% of observations should lie within $\pm\,\Delta$ (confidence interval) of the set of observations. Equation 3.35 shows the calculation of the confidence interval using the Student's t-method [37]:

$$\Delta\,(confidence\ interval\ at\ 95\%) = \frac{t_{n-1}S}{\sqrt{n}} \qquad (3.35)$$

where t_{n-1} is the t-value for the population samples having a size of *n* samples and a sample standard deviation of S. The precision uncertainty is defined as the calculated $\pm\,\Delta$ (confidence interval) for the set of observations. The percentage uncertainty is determined by comparing the calculated value with the mean of the observations. The precision uncertainty for the non-ultrasonic supercooling experiments was determined to be ±6.7% using the above method. Therefore, the total uncertainty is the root sum of squares of the bias and precision uncertainties associated with a measured variable as defined by Equation 3.36:

$$U_{total} = \sqrt{(U_{bias})^2 + \left(U_{precision}\right)^2} \tag{3.36}$$

CHAPTER 4

RESULTS AND DISCUSSION

A set of preliminary non-ultrasound (NUS) and ultrasound (US) experiments was performed to observe the supercooling effect in water and properly understand the appropriate application of ultrasound to improve this process. Figure 4.1 shows the list of experiments conducted as an initial study to assess and determine the topics that required further attention. The total energy consumption is indicated for each type of experiment as a summation of the cooling energy input and ultrasonic energy input. The error lines indicate the bias uncertainties associated with the specific type of experiment. As these were preliminary experiments, iterative experiments were not conducted, therefore a precision uncertainty could not be established for these trials.

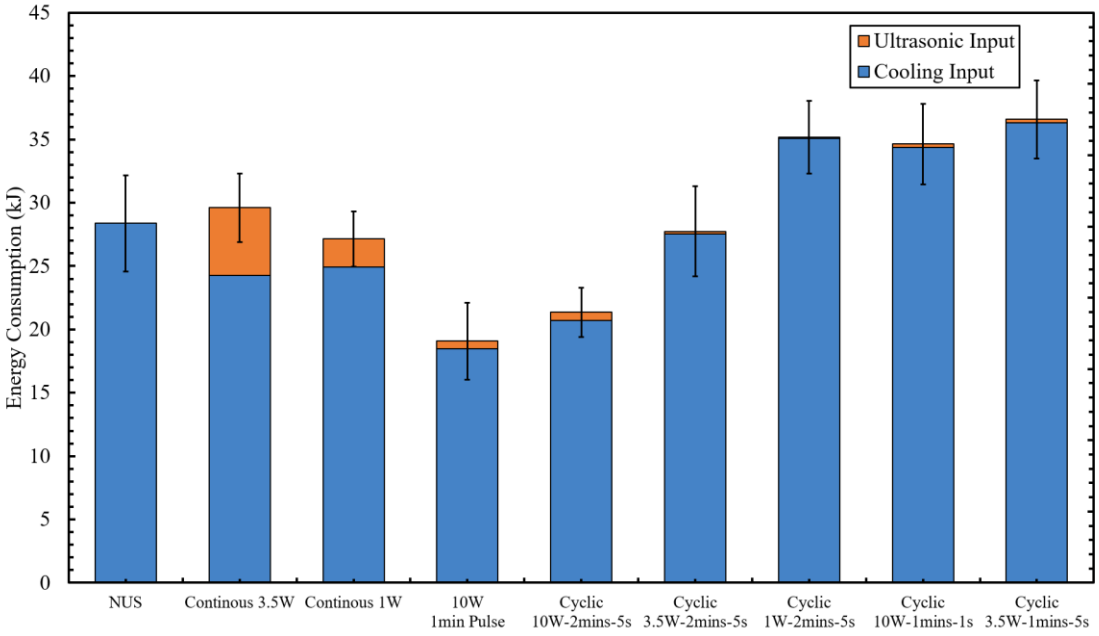

Figure 4.1: Preliminary experiments conducted at higher flow rate (error lines showing bias uncertainties associated with the experiments).

Figure 4.1 documents the energy consumption data for the different types of experiments that were conducted such as Non-Ultrasound experiments (NUS), Continuous ultrasonic experiments, Pulsed ultrasonic experiments, and Cyclic ultrasonic experiments. These experiments were conducted at a higher flow rate of 0.0161 kg/s which helped reduce the overall freezing time of the experiments but also reduced the overall ΔT (temperature difference) between the inlet and outlet temperatures of the coolant which resulted in a higher uncertainty. The non-ultrasound experiments are simple freezing experiments without the application of ultrasound, mainly conducted to observe the supercooling phenomenon and act as an energy consumption baseline for other experiments. In the ultrasonic experiments, ultrasound is only applied during the phase change process wherein the temperature of the water stagnates at 0 °C. *Continuous Ultrasonic* experiments refers to the constant sonication during the freezing process which is inherently inefficient due to excess energy consumption and heat dissipation of the acoustic energy. *Pulsed* experiments are the one-time application of ultrasound which is used to initiate the nucleation of ice at the beginning stages of supercooling when the water temperature dips below 0 °C. *Cyclic* experiments are optimized experiments wherein ultrasound was applied for a short time period and repeated at given intervals to maintain the ultrasonic effect over the course of the entire freezing process for a low overall energy consumption. For example, 10W of ultrasound at 26kHz was applied every 2 minutes for a period of 5 seconds after temperatures reached 0 °C until the freezing process was completed which was indicated by the temperatures dipping below 0 °C. From the various experiments shown in Figure 4.1, the pulsed and cyclic type experiments with 10W showed lower energy consumption

rates when compared with the other experiments. Therefore, further experiments were focused on these conditions to obtain greater energy enhancements.

4.1. Supercooling in Water

Since the non-ultrasound experiments are considered as baseline experiments in terms of energy consumption, it is important to properly understand the underlying phenomena occurring in the process. Figure 4.2 showcases the thermocouple readings inside the water during the non-ultrasound experiment.

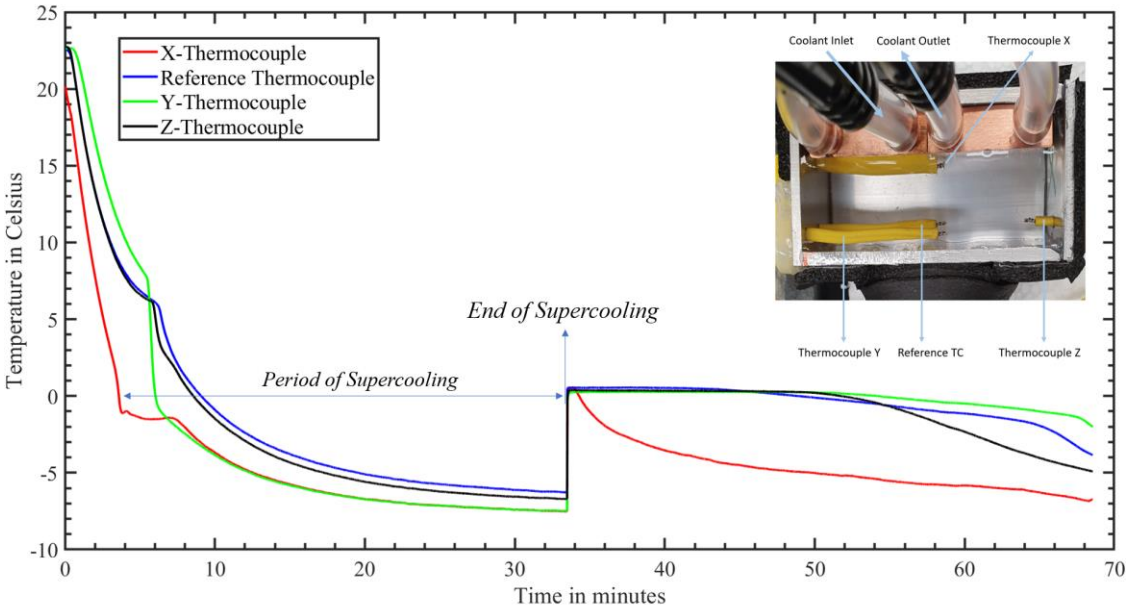

Figure 4.2: Thermocouple readings for non–ultrasound experiment

It can be observed that the thermocouple temperature readings start to dip below 0 °C around 4 minutes into the experiment which signifies the start of supercooling. During the supercooling period, the undisturbed water remains stagnant and in a liquid state even as the temperatures continue to decrease. At a certain temperature threshold around −7.5 °C at approximately the 34th minute, an instant freezing phenomenon occurs which results in a sudden jump in the temperatures to just above 0 °C. The freezing phenomenon results in

the formation of ice slurries or ice-water mixture which cannot be classified as a complete solid or liquid structure as the formed ice crystals are unstable and quickly melt back into water. After this point, the freezing process continues at a steady rate with solid ice being formed from the side of the copper cooling blocks. The temperatures at the different thermocouples stagnate at 0 °C until the ice formation reaches the locations of the specific thermocouples which results in a temperature drop.

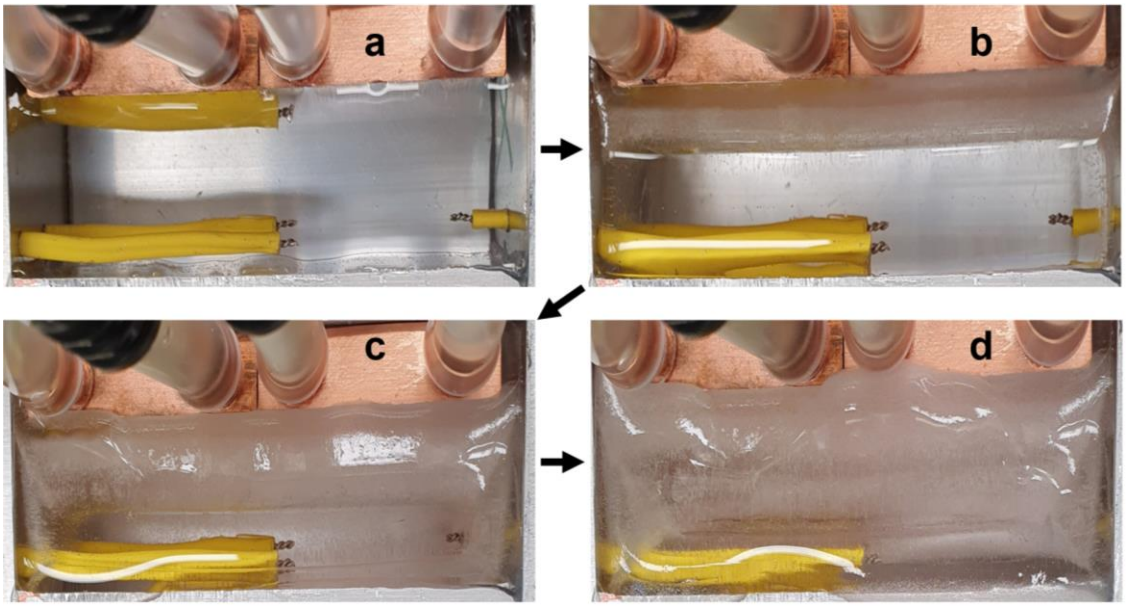

Figure 4.3: Formation of ice layer during the experiment: (a) No ice at the start of the experiment (b) Ice covering X-thermocouple (c) Ice covering Z-thermocouple (d) Ice covering Y and Reference Thermocouple

For example, the X-thermocouple temperature is the first to drop below 0 °C at the 35^{th} minute as it is closest to the copper cooling blocks, and therefore is frozen earlier than the other thermocouples as seen in Figure 4.3.b. Gradually the Z-thermocouple reading eventually drops in temperature as it undergoes freezing as indicated by Figure 4.3.c. Finally freezing takes place at the Y and reference thermocouple locations. The experiment is stopped when the last thermocouple drops down to a temperature of -2 °C which is

indicated by the Y-thermocouple reading in this particular case as shown in Figure 4.2. The coolant inlet and outlet temperature differences are measured over the course of the experiment as shown in Figure 4.4.

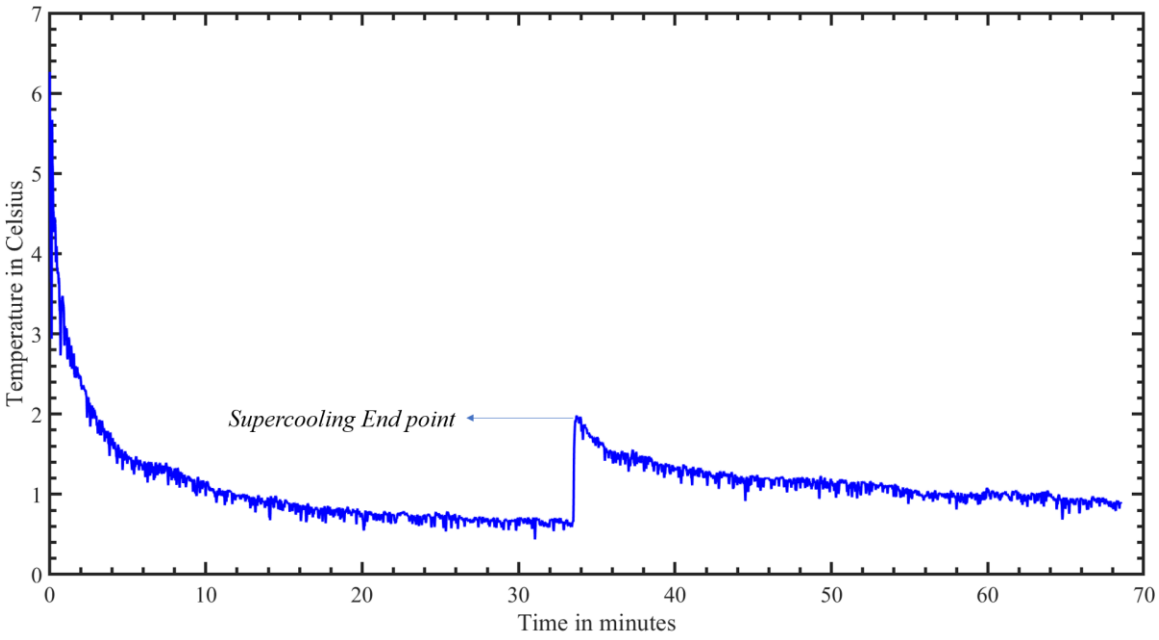

Figure 4.4: Coolant inlet & outlet temperature difference (ΔT) in non-ultrasound experiment

It can be observed that ΔT steadily reduces during the supercooling period but there is a sudden rise in the ΔT corresponding to the instant freezing phenomenon that occurs at the end point of the supercooling period. This increase in ΔT can be attributed to the sudden temperature rise observed in Figure 4.2 and the latent heat energy absorbed by the water during the instant freezing process. After the sudden peak in ΔT, the temperature differences again begin to reduce steadily. The measured ΔT values are used in the energy consumption calculations for the experiment as specified by Equation 3.1 and Equation 3.31.

The extent of supercooling of water has been observed to occur at varying temperatures by several researchers [15]&[17]. Therefore, the non-ultrasound freezing experiment was repeated several times under the same conditions to properly understand the range of temperatures over which supercooling occurs. Figure 4.5 showcases the repeated non-ultrasound experimental trials and the maximum temperatures observed during the supercooling phenomenon for each trial. The error bars indicate the total uncertainties at the 95% confidence level associated with the trials. The cleaning conducted prior to the specific experimental trails are also indicated. These experiments were conducted at a lower flow rate of 0.0043 kg/s to ensure better ΔT (i.e., higher) values which helps reduce the uncertainties in the measurements.

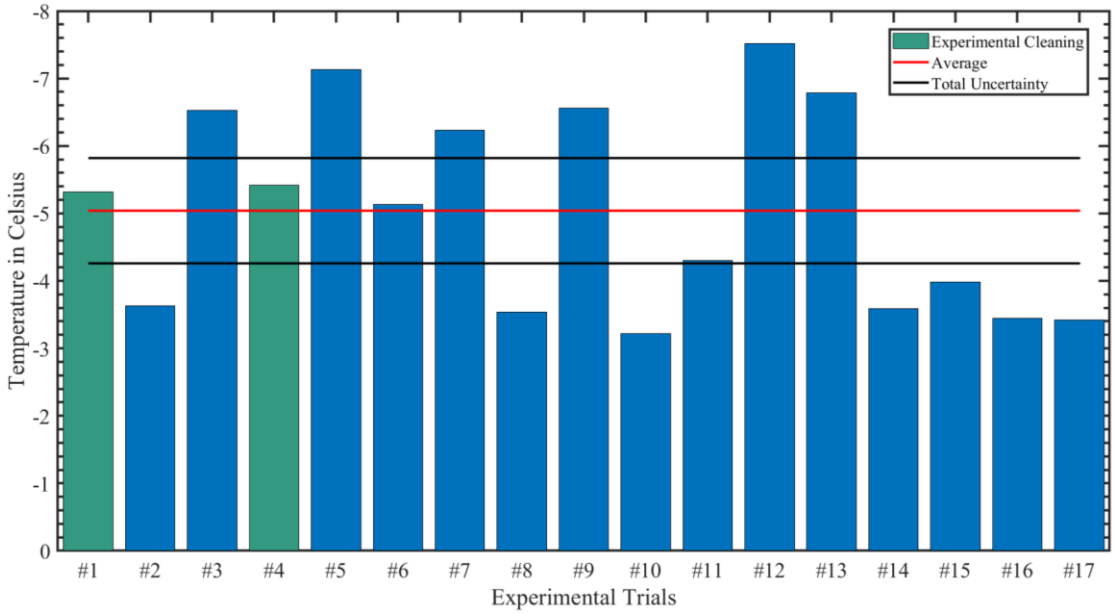

Figure 4.5: Maximum temperature of supercooling (lower flow rate experiments) with green bars indicating cleaning conducted prior to experimental trials

From Figure 4.5, it is noticeable that for the various consecutive experiments that were conducted, there is substantial variability in the maximum temperature of supercooling and this has also been observed by several other researchers [15], [17], [19]. This variability

increases the precision uncertainty for the energy consumption measurement. In order to further understand the relationship between the degree of supercooling and the overall energy consumption, Figure 4.6 was prepared wherein the energy consumption data for the set of non-ultrasound experiments were arranged in descending order and compared with their corresponding periods of supercooling. The period of supercooling is directly proportional to the maximum temperature of supercooling due to the longer cooling periods required for reaching lower temperatures.

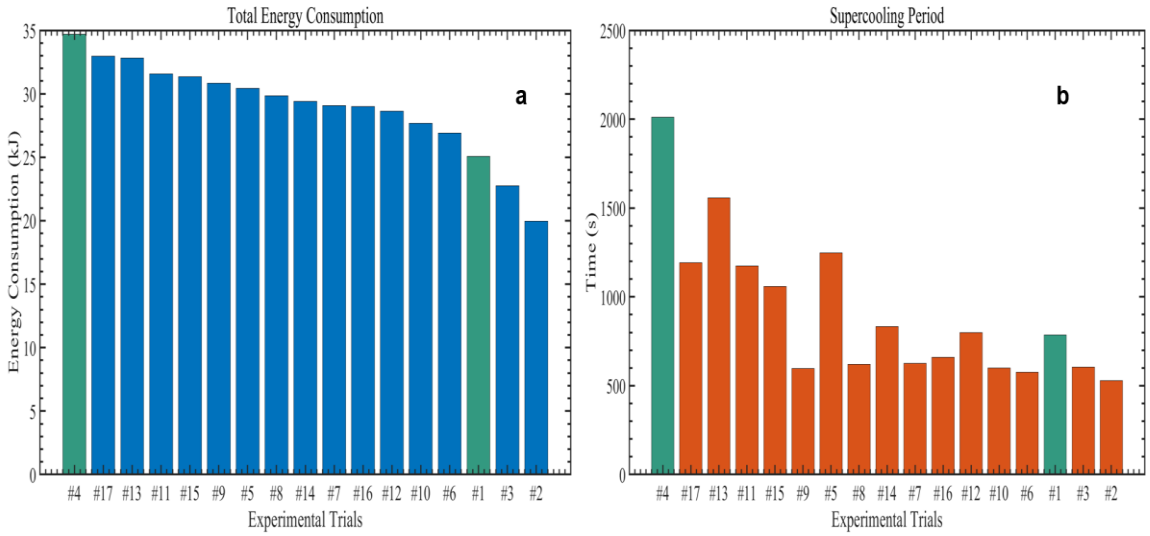

Figure 4.6: Descending order of energy consumption (a) and corresponding supercooling period (b) for non-ultrasonic experiments (green bars indicating cleaning conducted prior to experimental trials)

By comparing the graphs in Figure 4.6.a and 4.6.b, it can be observed that there is a potential trend which indicates that energy consumption increases with greater supercooling periods. Therefore, it can be interpreted that by reducing the overall supercooling period during the freezing process, there is a potential energy savings possibility which can be achieved using the application of ultrasound.

4.2. Effect of Ultrasound on Supercooling and Freezing Phenomenon

After establishing the supercooling effect in the freezing process of water and testing the preliminary ultrasonic experiments, the optimized cyclic 10W and 3.5W ultrasonic experiments were further investigated. The experiments were conducted using a lower flow rate of 0.0043 kg/s. In order to better represent the energy data in a practical setting, a Coefficient of Performance (COP) is considered for the calculated energy consumption data to emulate the energy performance of an actual ice machine. A COP was chosen for the current calculations based on the research done by Yashar et al. who proposed that a reasonable value for the COP for an energy analysis of ice machines was 1.8 [4]. Therefore, the calculated energy consumption data in this section have been adjusted after accounting for the COP value. Primarily in the ultrasonic experiments, sonication initiated the nucleation of ice which can be attributed to cavitation effects as reported by several others in Chapter 1. The extended usage of ultrasound was done to promote microjet and microstreaming phenomena that reportedly improved heat transfer in liquids [10]. A cyclic ultrasonic experiment was conducted with 10W-26kHz ultrasound applied every 2 minutes for a duration of 5 seconds. Figure 4.7 shows the thermocouple temperature readings for the experiment. The ultrasound is applied when the water temperature reaches 0 °C. X-thermocouple shown in Figure 4.7 is the first thermocouple to reach 0 °C at the 3rd minute of the experiment, at which point 10W of ultrasound is applied for a duration of 5 seconds. Immediately after ultrasound is first applied, a sudden temperature rise is observed in the X-thermocouple reading. This is attributed to the freezing process that produces ice at the surface of the cooling blocks and at the location of the X-thermocouple. This indicates that freezing was successfully initiated using ultrasound and supercooling of water was eliminated.

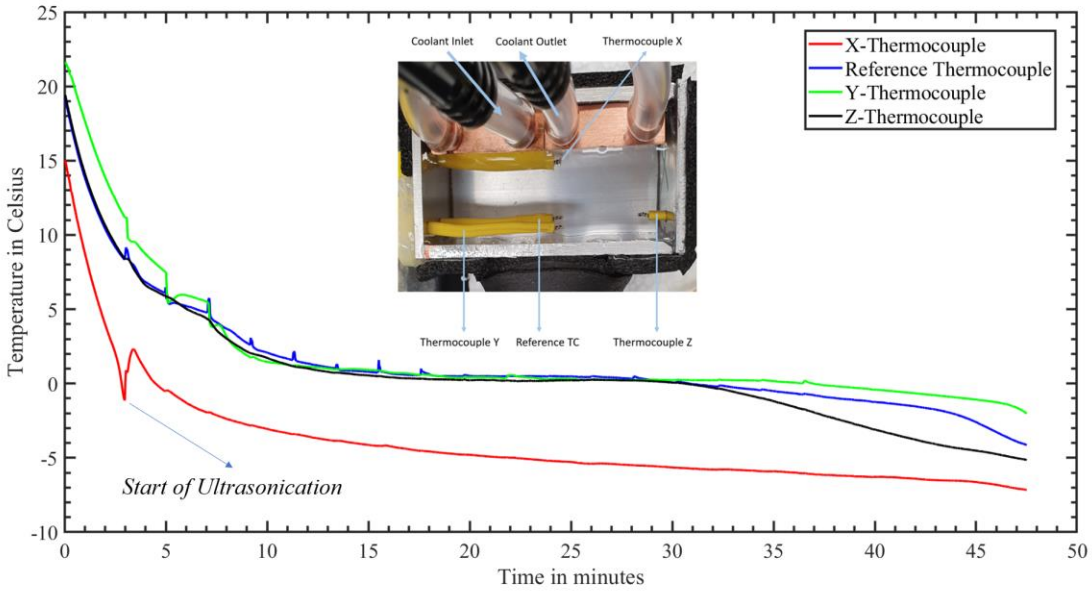

Figure 4.7: Thermocouple readings for cyclic 10W-26kHz ultrasound experiment

After the formation of an initial solid layer of ice, supercooling does not occur at any other point inside the water domain as the solid ice layer acts as a nucleation seed point for the generation of further ice crystals as explained by Dorsey [6]. Therefore, as the experiment continued, the other thermocouple temperatures approached 0 °C but did not dip below 0 °C. Ultrasound was consistently applied for a duration of 5 seconds every 2 minutes until the last thermocouple reading dropped below 0 °C, after which the application of ultrasound was stopped. The formation of ice layer in the water domain is similar to the non-ultrasound case as explained previously using Figure 4.3. As the Reference thermocouple is placed closest to the ultrasonic transducer, the cyclic application of ultrasound results in a slight temperature rise at the Reference thermocouple location which can be noticed by the minor peaks in the temperature measurements at the initial stages of the experiment. Figure 4.8 shows the temperature difference (ΔT) between the inlet and outlet temperatures for the coolant for the 10W cyclic ultrasonic experiment.

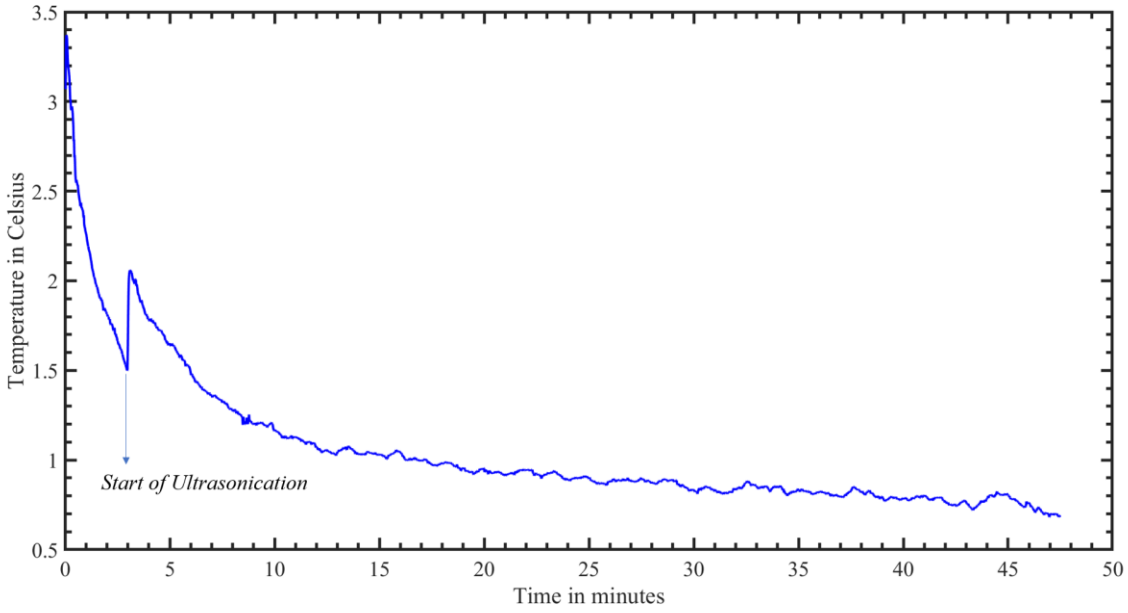

Figure 4.8: Coolant inlet & outlet temperature difference (ΔT) in 10W-26kHz cyclic ultrasound experiment

As observed in Figure 4.8, the start of ultrasonication results in a sudden jump in ΔT which can be attributed to the freezing initiated by the ultrasonic waves. After an initial rise in ΔT, it steadily reduces over the course of the experiment. A similar graphical trend is observed in the temperature measurements for the 3.5W-26kHz cyclic ultrasound experiments which proves that ultrasound applied at 3.5W also helps in initiating freezing and eliminating supercooling in water which allows a lower energy consuming option for ultrasonic application. Figure 4.9 shows a comparison of the temperature measurements between the non-ultrasound and 10W cyclic experiment for the Y-thermocouple readings.

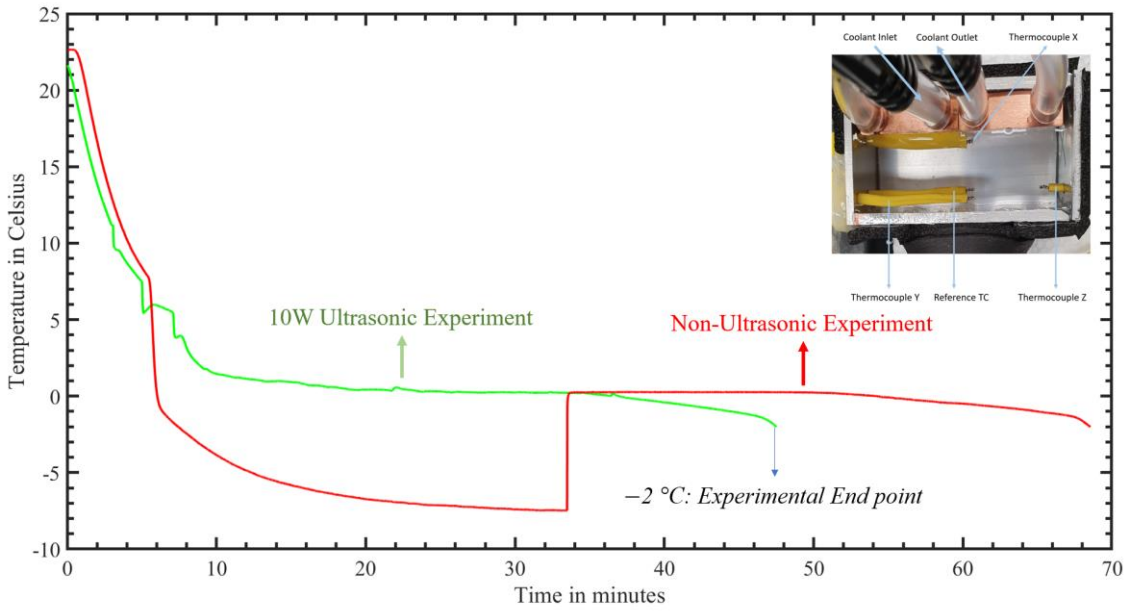

Figure 4.9: Comparison of Y-thermocouple readings between 10W cyclic and non-ultrasound experiment

There is a noticeable difference in the end points for the experiments which indicates that the cyclic ultrasound experiment significantly reduces the overall duration of the freezing process. This also contributes to the reduction in energy consumption for the ultrasonic experiments.

During the cyclic ultrasound experiments, a unique phenomenon was observed. As the experiment proceeded, ice shards/crystals were found stagnating inside the water domain during the ultrasonic experiments. Figure 4.10 shows the captured images of ice crystals/shards that were found in the 10W and 3.5W experiments which are compared with an image of a non–ultrasound experiment taken at an equivalent time. It was also visually observed that the concentration and size of the crystals differed between the 10W and 3.5W experiments, wherein there was a greater concentration and size of ice crystals

observed in the 10W ultrasonic experiments. This is a potentially interesting topic that could be explored in future work.

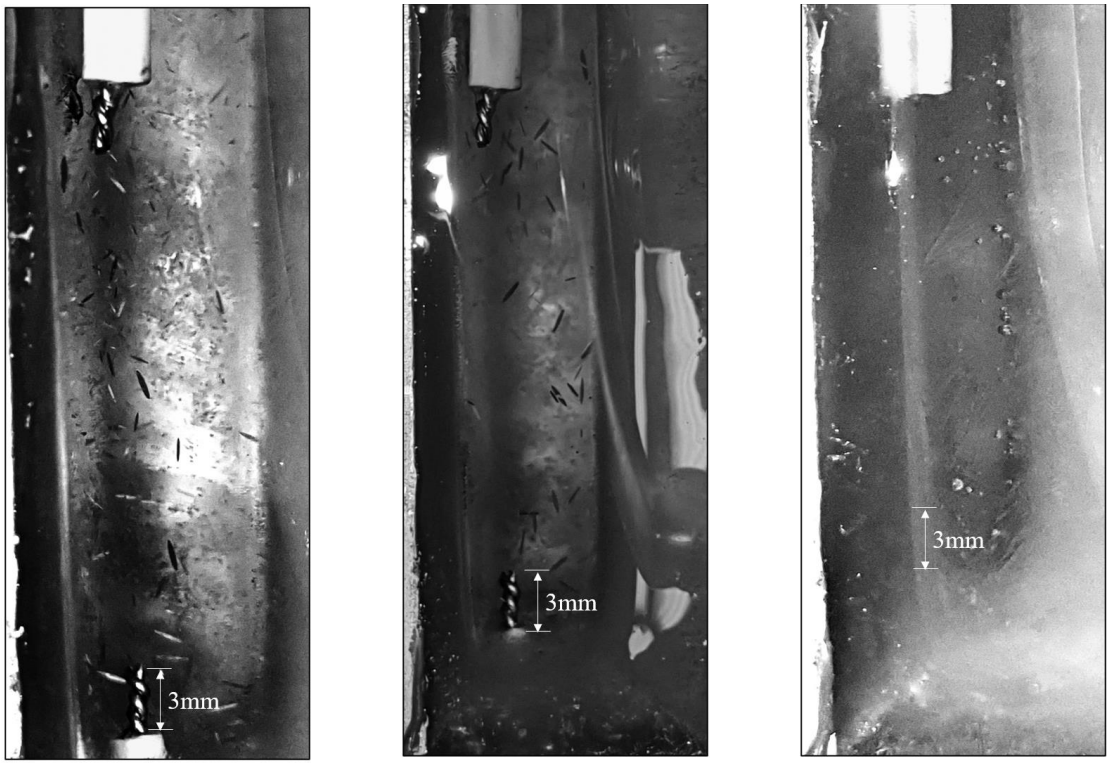

Figure 4.10: Presence of ice crystals in the 10W cyclic (left image), 3.5W cyclic (middle image) and absence of crystals in the non-ultrasound experiment (right image).

The non-ultrasound experiments and the cyclic 10W & 3.5W experiments were repeated to observe variations in the energy consumption data. Figure 4.11 shows the energy analysis data for the various experiments. All the different types of experiments show a large variability between the maximum and minimum values. The total uncertainties of the respective energy consumption data at the 95% confidence level are displayed as the error lines on the average measurements for each of the experiments. The variability in the energy measurements for the non-ultrasonic experiments is attributed to the unpredictable nature of supercooling. The energy consumption in the ultrasonic experiments also

produces results with a degree of variability. It could be said that the unpredictable nature of the supercooling phenomenon in the non-ultrasound experiments can be attributed to interactions of the impurities in the tap water sample. A similar explanation could be the cause for the variation in the results for the ultrasonic experiments. This would require further experimentation and study to understand the underlying principle.

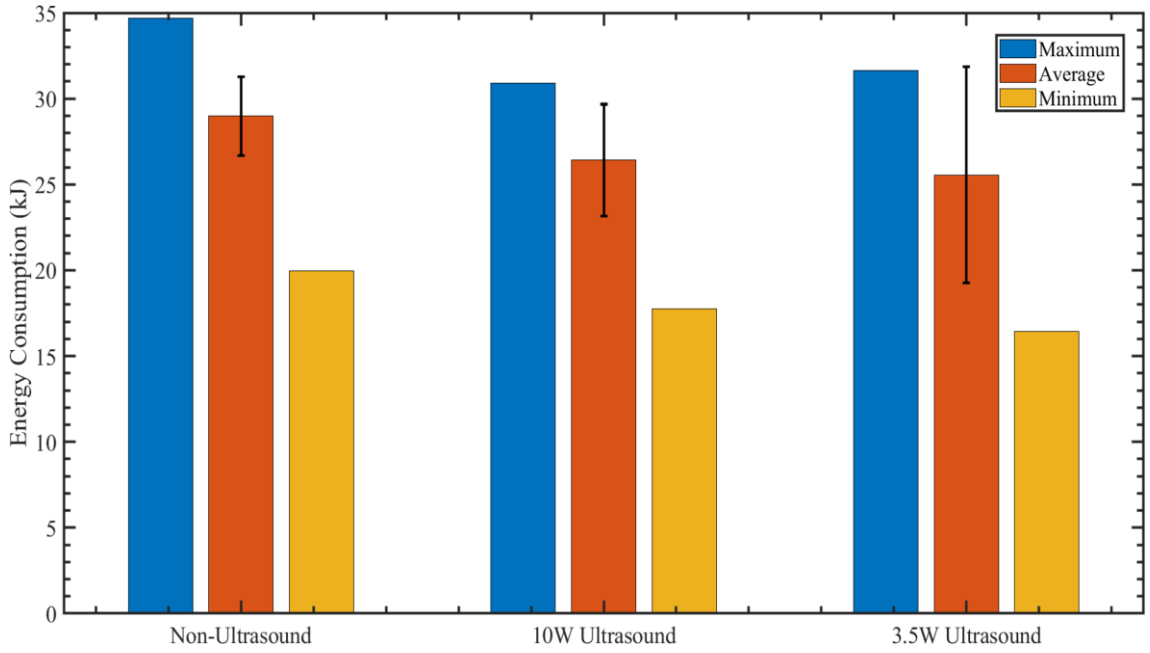

Figure 4.11: Energy consumption for various experiments (error line showing the total uncertainty associated with the respective experiments)

The variability in these experiments directly translates to a larger precision uncertainty value attributed to these measurements. Table 4.1 gives the total uncertainty calculated for the measured energy consumption values for the different experiments.

Table 4.1: Total uncertainty in the energy consumption value for various experiments.

Experimental Parameter	**Total Uncertainty Value**
Energy consumption in Non-Ultrasound Experiment	±7.9 %
Energy consumption in 10W Ultrasound Experiment	±12.4 %
Energy consumption in 3.5W Ultrasound Experiment	±24.6 %

Therefore, after accounting for the total uncertainties in various experiments, Figure 4.12 shows the Ultrasonic Enhancement (UE) for the 10W and 3.5W cyclic experiments. The Ultrasonic Enhancement parameter defined in Equation 4.1 was used to present the percentage energy efficiency achieved by using ultrasound when compared with the non-ultrasound experiments:

$$UE = \frac{E - E_{US}}{E} \times 100\ \% \tag{4.1}$$

where E is the energy consumption for the non-ultrasonic experiments and E_{US} the energy consumption in the specific type of ultrasonic experiment.

The ultrasonic power intensities used in this study were 0.22 $W\ cm^{-2}$ and 0.07 $W\ cm^{-2}$. The average cooling power intensity applied for the non-ultrasound experiments were 0.33 $W\ cm^{-2}$. This indicates that the lower ultrasonic power intensity is a feasible option for enhancement applications when compared with the cooling power intensity.

It is seen in Figure 4.12 that the achieved energy enhancements are largely within the uncertainty boundaries. Although this is cause for concern as an overall result, it does not disqualify the achieved energy enhancement results. The large uncertainties that were found can be attributed to the variable nature of the experiment itself.

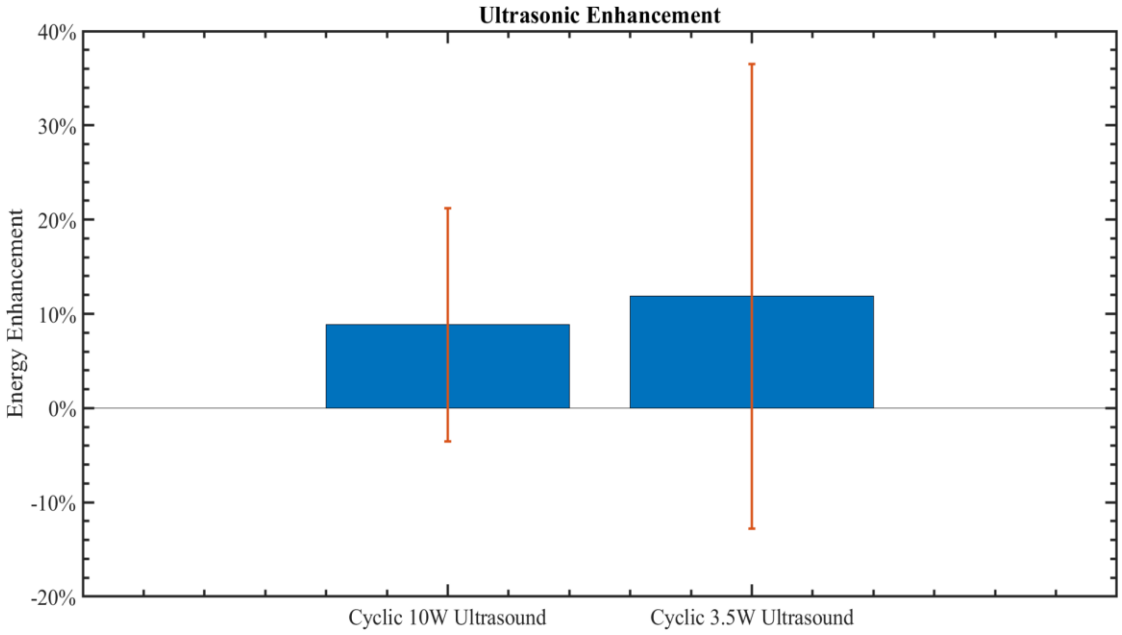

Figure 4.12: Ultrasonic Enhancement for Cyclic 10W & 3.5W Experiments (Error bars indicating the total uncertainty in the measurement)

As per the Student's t-method of precision uncertainty calculation given by Equation 3.34, where t_{n-1} is the t-value for the population samples having a size of *n* samples and a sample standard deviation of *S*, by increasing the number of runs or samples *n* for a given experiment, the overall uncertainties for the measurements can possibly be reduced. Therefore, although the current uncertainties attributed to the experiment are large, they are not yet definitive. The energy enhancement gained for the 10W and 3.5W cyclic experiments in comparison with the non-ultrasound experiments are shown in Table 4.2.

Table 4.2: Ultrasonic Energy Enhancement Achieved

Experiment	**Ultrasonic Enhancement (UE)**
10W Cyclic Ultrasound Experiment	8.9% ± 12.4%
3.5W Cyclic Ultrasound Experiment	11.9 % ± 24.6%

CHAPTER 5

CONCLUSION

In this study, the effect of ultrasound on the supercooling and freezing processes of water was investigated. After a set of preliminary experiments, an optimized set of cyclic ultrasonic experiments was found to be promising and was investigated in further detail. It was determined that the application of ultrasound helped to eliminate supercooling in water and initiate ice nucleation.

Several iterative runs of non-ultrasound freezing experiments were conducted to properly observe and measure the variable nature of the supercooling effect in water. A possible trend was discovered indicating a potential relationship between cooling energy consumption and period/degree of supercooling.

The application of ultrasound helped reduce the overall duration of the freezing process. It was also observed that the effect of ultrasonic waves during the freezing process resulted in the formation of ice crystals/shards. The ultrasonic experiments were focused on the 10W and 3.5W cyclic ultrasonic experiments which resulted in an overall energy enhancement of 8.9% ± 12.4% and 11.9 % ± 24.6%, respectively.

CHAPTER 6

FUTURE SCOPE

The current study was conducted to improve the heat transfer and phase change process of freezing water. Although the positive effect of ultrasound was established, more study is required to understand the underlying principles occurring during this process. Firstly, a greater number of ultrasonic experiments are needed to be run in order to properly establish the efficiency enhancements beyond the uncertainty bounds. The current experiments were conducted for an ultrasonic frequency of 26 kHz. Therefore, the effects of higher frequency ultrasonic waves must also be investigated. Only 2 main power levels of 10W and 3.5W were studied in this experiment which provides the opportunity to explore higher or lower power input levels to the ultrasonic transducer.

The current experiment was conducted as an open system wherein the top surface was exposed to external interactions. Any further experimentations conducted should be considered as a fully insulated system to measure the thermal conditions more accurately. The heat transfer medium and the coolant can also be modified to emulate industrial settings to achieve better practical results.

REFERENCES

[1] William Goetzler et al.., “Energy Savings Potential and Research & Development Opportunities for Commercial Refrigeration,” DOE/EE--0847, 1219982, Sep. 2009. doi: 10.2172/1219982.

[2] “Ice Manufacturing: 2002 2002 Economic Census Manufacturing Industry Series Issued.” Dec. 2004.

[3] D. Fisher, D. Cowen, A. Karas, and C. Spoor, “Commercial Ice Machines: The Potential for Energy Efficiency and Demand Response,” ©2012 ACEEE Summer Study Energy Effic. Build., vol. 9–103, p. 12.

[4] D. A. Yashar and K.-J. Park, “Energy Consumption of Automatic Ice Makers Installed in Domestic Refrigerators,” NIST Tech. Note 1697, [Online]. Available: https://www.nist.gov/publications/energy-consumption-automatic-ice-makers-installed-domestic-refrigerators-nist-tn-1697.

[5] H. Zhao, F. Zhang, H. Hu, S. Liu, and J. Han, “Experimental study on freezing of liquids under static magnetic field,” Chin. J. Chem. Eng., vol. 25, no. 9, pp. 1288–1293, Sep. 2017, doi: 10.1016/j.cjche.2016.10.026.

[6] N. E. Dorsey, “The Freezing of Supercooled Water,” Trans. Am. Philos. Soc., vol. 38, no. 3, p. 247, Nov. 1948, doi: 10.2307/1005602.

[7] P. Wilson, Ed., Supercooling. InTech, 2012.

[8] “VIII. Experimenta & observationes de congelatione aquæ in vacuo factæ a D. G. Fahrenheit, R. S. S,” Philos. Trans. R. Soc. Lond., vol. 33, no. 382, pp. 78–84, Dec. 1724, doi: 10.1098/rstl.1724.0016.

[9] D. Ensminger and L. J. Bond, Ultrasonics: fundamentals, technologies, and applications, 3rd ed. Boca Raton, FL: Taylor & Francis, 2012.

[10] M. Legay, N. Gondrexon, S. Le Person, P. Boldo, and A. Bontemps, “Enhancement of Heat Transfer by Ultrasound: Review and Recent Advances,” Int. J. Chem. Eng., vol. 2011, pp. 1–17, 2011, doi: 10.1155/2011/670108.

[11] L. Bjørnø, “Finite-Amplitude Waves,” in Applied Underwater Acoustics, Elsevier, 2017, pp. 857–888.

[12] E. A. Neppiras, “Acoustic cavitation,” Phys. Rep., vol. 61, no. 3, pp. 159–251, May 1980, doi: 10.1016/0370-1573(80)90115-5.

[13] M. Dalvi-Isfahan, N. Hamdami, E. Xanthakis, and A. Le-Bail, “Review on the control of ice nucleation by ultrasound waves, electric and magnetic fields,” J. Food Eng., vol. 195, pp. 222–234, Feb. 2017, doi: 10.1016/j.jfoodeng.2016.10.001.

[14] F. Baillon, F. Espitalier, C. Cogné, R. Peczalski, and O. Louisnard, “Crystallization and freezing processes assisted by power ultrasound,” in Power Ultrasonics, Elsevier, 2015, pp. 845–874.

[15] T. Inada, X. Zhang, A. Yabe, and Y. Kozawa, “Active control of phase change from supercooled water to ice by ultrasonic vibration 1. Control of freezing temperature,” Int. J. Heat Mass Transf., vol. 44, no. 23, pp. 4523–4531, Dec. 2001, doi: 10.1016/S0017-9310(01)00057-6.

[16] X. Zhang, T. Inada, A. Yabe, S. Lu, and Y. Kozawa, “Active control of phase change from supercooled water to ice by ultrasonic vibration 2. Generation of ice slurries and effect of bubble nuclei,” Int. J. Heat Mass Transf., vol. 44, no. 23, pp. 4533–4539, Dec. 2001, doi: 10.1016/S0017-9310(01)00058-8.

[17] T. Hozumi, A. Saito, S. Okawa, and T. Matsui, “Freezing phenomena of supercooled water under impacts of ultrasonic waves,” Int. J. Refrig., vol. 25, no. 7, pp. 948–953, Nov. 2002, doi: 10.1016/S0140-7007(01)00104-9.

[18] X. Zhang, T. Inada, and A. Tezuka, “Ultrasonic-induced nucleation of ice in water containing air bubbles,” Ultrason. Sonochem., vol. 10, no. 2, pp. 71–76, Mar. 2003, doi: 10.1016/S1350-4177(02)00151-7.

[19] R. Chow, R. Blindt, R. Chivers, and M. Povey, “A study on the primary and secondary nucleation of ice by power ultrasound,” Ultrasonics, vol. 43, no. 4, pp. 227–230, Feb. 2005, doi: 10.1016/j.ultras.2004.06.006.

[20] A. Olmo, R. Baena, and R. Risco, “Use of a droplet nucleation analyzer in the study of water freezing kinetics under the influence of ultrasound waves,” Int. J. Refrig., vol. 31, no. 2, pp. 262–269, Mar. 2008, doi: 10.1016/j.ijrefrig.2007.05.012.

[21] R. Chow, R. Blindt, R. Chivers, and M. Povey, “The sonocrystallisation of ice in sucrose solutions: primary and secondary nucleation,” Ultrasonics, vol. 41, no. 8, pp. 595–604, Nov. 2003, doi: 10.1016/j.ultras.2003.08.001.

[22] L. F. Cabeza, H. Mehling, S. Hiebler, and F. Ziegler, “Heat transfer enhancement in water when used as PCM in thermal energy storage,” Appl. Therm. Eng., vol. 22, no. 10, pp. 1141–1151, Jul. 2002, doi: 10.1016/S1359-4311(02)00035-2.

[23] Y. Liu, X. Li, P. Hu, and G. Hu, “Study on the supercooling degree and nucleation behavior of water-based graphene oxide nanofluids PCM,” Int. J. Refrig., vol. 50, pp. 80–86, Feb. 2015, doi: 10.1016/j.ijrefrig.2014.10.019.

[24] W. Cui, L. Jia, Y. Chen, Y. Li, J. Li, and S. Mo, “Supercooling of Water Controlled by Nanoparticles and Ultrasound,” Nanoscale Res. Lett., vol. 13, no. 1, p. 145, Dec. 2018, doi: 10.1186/s11671-018-2560-z.

[25] L. S. Jia, W. Cui, Y. Chen, Y. A. Li, and J. Li, “Effect of ultrasonic power on super-cooling of TiO2 nanoparticle suspension,” Int. J. Heat Mass Transf., vol. 120, pp. 909–913, May 2018, doi: 10.1016/j.ijheatmasstransfer.2017.12.128.

[26] Y. Liu et al.., “The effects of graphene oxide nanosheets and ultrasonic oscillation on the supercooling and nucleation behavior of nanofluids PCMs,” Microfluid. Nanofluidics, vol. 18, no. 1, pp. 81–89, Jan. 2015, doi: 10.1007/s10404-014-1411-1.

[27] Z. Yan, Z. (Jerry) Yu, T. Yang, S. Li, and G. Zhang, “Impact of ultrasound on the melting process and heat transfer of phase change material,” Energy Procedia, vol. 158, pp. 5014–5019, Feb. 2019, doi: 10.1016/j.egypro.2019.01.663.

[28] X. Cheng, M. Zhang, B. Xu, B. Adhikari, and J. Sun, “The principles of ultrasound and its application in freezing related processes of food materials: A review,” Ultrason. Sonochem., vol. 27, pp. 576–585, Nov. 2015, doi: 10.1016/j.ultsonch.2015.04.015.

[29] L. Zheng and D.-W. Sun, “Innovative applications of power ultrasound during food freezing processes—a review,” Trends Food Sci. Technol., vol. 17, no. 1, pp. 16–23, Jan. 2006, doi: 10.1016/j.tifs.2005.08.010.

[30] “AP/Armaflex Insulation Tape Datasheet.” [Online]. Available: https://www.armacell.us/fileadmin/user_upload/Reference_Sheets_INS/AP_ArmaFlex_Roll_and_Sheet_Tolerances_and_R-Values.EN.US.2019.pdf.

[31] “Engineering and Operating Guide for DOWTHERM SR-1 and DOWTHERM 4000 Inhibited Ethylene Glycol-based Heat Transfer Fluids.” DOWTHERM, [Online]. Available: https://www.dow.com/content/dam/dcc/documents/en-us/app-tech-guide/180/180-01190-01-engineering-and-operating-guide-for-dowtherm-sr1-and-dowtherm-4000.pdf?iframe=true.

[32] K. S. Ong, L. Jiang, and K. C. Lai, “4.20 Thermoelectric Energy Conversion,” in Comprehensive Energy Systems, Elsevier, 2018, pp. 794–815.

[33] E. Dasinor, “Thermal Resistance Measurements of Triply Periodic Minimal Surface Structures (TPMS) of the Thermogalvanic Brick.” Arizona State University.

[34] R. Park et al.., Manual on the Use of Thermocouples in Temperature Measurement, Fourth Edition, Sponsored by ASTM Committee E20 on Temperature Measurement, 4TH ed. ASTM International, 1993.

[35] W. Bertrand, “Enhanced Desorption in Novel Sorbent Materials Using Ultrasound.” Arizona State University.

[36] Y. A. Çengel and A. J. Ghajar, Heat and mass transfer: fundamentals & applications, Fifth edition. New York, NY: McGraw Hill Education, 2015.

[37] J. P. Holman, Experimental methods for engineers, 8th ed. Boston: McGraw-Hill/Connect Learn Succeed, 2012.